Modelling of a battery energy storage system in a low voltage distribution grid with high photovoltaic (PV) penetration.

EG59F2 Individual Project in Renewable Energy Engineering

By

Keron Mark Denny, B.Eng., MBA.

50075314

A dissertation submitted in partial fulfilment of the requirements of the award of Master of Science in Renewable Energy Engineering at the University of Aberdeen

(November 2023)

Abstract

In Norway, the landscape of energy generation has evolved significantly during the past decade, and this will further increase in the coming years. This new type of energy generation refers to distributed energy resources (DERs) providing electrical power to the grid. In Norway, residential photovoltaic (PV) systems are the most dominant source.

PV installations, especially in the low-voltage grid, can induce overvoltage complications arising from substantial solar energy production. This dissertation investigated this challenge and examined the efficacy of a peak shaving control strategy to reduce voltage rise via the use of a Battery Energy Storage System (BESS).

Simulations were conducted using MATLAB Simulink, wherein each consumer's home was hypothetically installed with 16.3 kW PV system which is also integrated to the grid. Voltage rise in the grid was first observed via load flow analyses, which served as the foundation for subsequent investigations using irradiance and load demand data for 18th April 2022 of a location in Norway.

During these simulations with the aggregated PV production, it showed that when there was high PV production with low load demands, the grid could not maintain the voltage variations within the specified acceptable limits. During the dissertation it was also noted that due to the high R/X ratios of the overhead lines, over voltages would continue to occur if no interventions are implemented.

A BESS integrated to the grid using a peak shaving control strategy was shown to reduce the voltage variations within the specified limits and illustrated its flexibility to supply other services as well.

During this simulation it was found that the BESS reduced the grid voltage from 1.11 pu to an acceptable value of approximately 1.08 pu during peak PV production, thus avoiding overvoltage occurrences.

This dissertation proved that the integration of a battery energy storage system provides an added approach to alleviating voltage rise due to high PV production.

Acknowledgements

First and foremost, I would like to give thanks to almighty God for giving me the strength and persistence to complete this course along with the completion of this dissertation. I would also like to thank my wife, Linda and my children Liam and Celin for their patience and understanding. Also, my stepson Marco, for helping more at home during this period thus enabling me to have more time to focus on this project.

From an academic standpoint, I would like to thank my academic supervisor,

Dr. Yifei Guo for providing superb guidance and for his willingness to push me to improve my simulations.

I would also like to thank my industrial supervisor, Dr. Bjørn Thorud for his insight and advice during this project. Through his thorough application of knowledge within the industry that was shared to me, it enabled me to understand and address current issues in Norway regarding DER integration.

Contents

List of Tables

List of Figures

List of symbols and notation

A	ampere
BESS	Battery Energy Storage System
BMS	Battery Management System
BTM	Behind the meter
DER	Distributed Energy Resource
DoD	Depth of discharge
DSO	Distribution service provider
EV	Electrical vehicle
F_{nom}	Nominal frequency
FTM	Front of the meter
Hrs	Hours
Hz	Hertz
HV	High voltage
IT	Isolated terra
kV	Kilovolt
kVa	kilovolt ampere
kWp	Kilowatt peak
kWh	kilowatt hour
L	Load
LV	Low voltage
MW	Megawatt
OLTC	On-load tap changer
P	Active power
PCC	Point of common coupling
Pu	Per unit
PV	Photovoltaic
Q	Reactive power
R	Resistance
S	Apparent power
SoC	State of charge
TN	Terra neutral
TN-C	Terra neutral combined
TN-C-S	Terra neutral combined separate
TN-S	Terra neutral separate
TSO	Transmission system operator
TT	Terra terra
TWh	Terrawatt hour
V	Voltage/Volt
W	watt
X	Reactance
Z	Impendence
Ω	Ohm
ϛ	Tap position
∆V	Voltage difference

1. Introduction

1.1 Background

The growth of Norwegian solar power development by the end of September 2023, was approximately 545 MW of solar energy from photovoltaic (PV) systems of which 250 MW were residential solar power generation connected to the electrical grid. Compared to Norway's total electrical installed production capacity of 42,571 MW this is not a large number, however, 72% of the solar PV installations were installed between 2022 and September 2023 according to data retrieved from Elhub which measures all the electrical distribution, consumption and production values in Norway [1] .This presents a significant growth, and the Norwegian Water Resources and Energy Directorate (NVE) has estimated that Norwegian solar energy installations could generate 7 TWh annually by 2030 [2].

Table 1.0 Installed solar capacity and other technologies.

Data translated by the author and taken from [1]

Total PV system installed capacity (2019 - Sept 2023)				**Other technologies**
Year	**Total (MW)**	**Private - Home and Cabins (MW)**	**C&I (MW)**	**MW**
2019	68.8	31.1	37.7	36857
2020	38.4	15.9	22.47	2681.9
2021	42.8	19.57	23.19	2194.9
2022	154	82.17	71.8	439.7
2023	241	100.82	140.3	397.5
Total accumulated (MW)	545.02	249.56	295.46	42571

Several grid companies express concern about the potential investment required for the distribution networks to accommodate this production. Traditionally, the Norwegian electrical grid is designed to transport electricity from large producing hydroelectric facilities, through high voltage (HV) transmission grids, medium voltage (MV) regional distribution grids and low voltage (LV) grids to finally reach

the end consumers [3]. However, this is changing with an increasing amount of distributed energy resources (DERs) being integrated in the power system.

Furthermore, the production from these sources fluctuates throughout the day and is directly related to weather variability [4] and as a result creates new demands on the design and operation of the grid.

In Norway, the current dominant DER in LV grids is residential photovoltaics (PV) systems and this trend will continue according to reference [2]. This dissertation will focus on a LV grid interaction with high PV penetration that causes associated voltage variations, creating overvoltage occurrences.

1.2 Motivation

The global energy landscape is rapidly evolving, with solar PV generation increasing to 270TWh in 2022 having an accumulative generation of 1300TWh according to reference [5]. This acceleration is fuelled by continuous technological advancements and the plummeting costs associated with solar installations [5]. In Norway, while PV systems have historically powered off-grid areas like remote cabins, the recent trend illustrates a surge in grid-tied PV systems. As residential PV systems become increasingly common place in Norwegian households, the conventional grid faces challenges, particularly, concerning grid stability such as reverse flow leading to voltage rise. In NVE's base scenario with 7 TWh production in 2040, it estimates approximately 215000 solar PV installation of various sizes will be distributed among residential homes [2].

With this significant predicted volume of PV installations, it will be essential to design low voltage grids systems that can be modified to include interventions methods that can effectively ensure reliability and sustainability by controlling the grid voltage. One such intervention is the use of a battery energy storage system (BESS).

1.3 Aims and objectives.

The purpose of this master dissertation is to prove that voltage rise in a low voltage distribution grid due to a high penetration of PV production can be alleviated using a BESS integrated in the grid. Furthermore, it aims to investigate how the BESS should be dimensioned and describes the control strategy used, as well as whether the BESS can provide any additional services when not needed for voltage regulation.

The dissertation aims are answered by achieving the following objectives:

- Developing a base case load flow analysis of the grid with consumers without PV integration and without BESS installation.
- Developing a load flow analysis of the grid with consumer with PV systems installed and integrated with the grid.
- Assessment of overvoltage occurrences.
- Developing a BESS modelling with the grid that has consumers with PV systems installed that are also integrated with the grid.
- Assessment of overvoltage alleviation with a BESS integration to the grid using a peak shaving control strategy.
- Brief overview of additional services the BESS can provide.

1.4 Approach

Based on these objectives, the approach was carried out and developed as follows:

- Design the grid in MATLAB's Simulink with and without 16.3 kW PV systems.
- Perform load flow analyses in Simulink of the grid without 16.3 kW PV systems at all consumers and record the voltage variations in per unit (pu).
- Perform load flow analyses in Simulink of the grid with 16.3 kW PV systems at each consumer and record the voltage variations in per unit (pu).
- In load data of ten (10) anonymized residential consumers in a low voltage (230 V IT) grid in Norway for modelling with and without the BESS.
- Perform a simulation of the grid using the aggregated load data from 22nd April, aggregated power of 163 kW from all PV systems and a BESS integrated in the grid using a peak shaving control strategy.
- Record and illustrate the performance of the BESS in its ability to reduce voltage rise.

1.5 Limitations

The ten (10) PV systems in this dissertation all have the same maximum power capacity of 16.3 kW, the size of the roofs is the same and large enough to install the capacity. The PV systems are installed on the roofs of residential private homes in the same rural area, with the same orientation. The solar panels have no shading losses and are assumed to be the same for all PV systems for ease of simulation. The battery modelling simulation will use aggregated load profiles and PV production of all consumers as to simplify the simulation and the BESS's installation will be done on the low voltage distribution grid, front of the meter (FTM). Also, no operating characteristics such as temperature of the BESS will

be included in this dissertation. Optimization of the PV control system is not reviewed, and reactive power management will not be discussed in this dissertation as BESS modelling for alleviation of voltage rise is the focus.

Other quality concerns such as harmonics and frequency will not be investigated but instead only the magnitudes of voltage variations with and without the BESS.

1.6 Dissertation scope

Chapter 1- **Introduction**: Gives a brief description of the background, motivation, aims, objectives, approach, and limitation and the dissertation scope.

Chapter 2 - **Background theory**: Provides the layout of the Norwegian power system with a focus on the distribution grid, documented theory regarding voltage control, battery energy system storage and peak shaving strategies.

Chapter 3 - **Methodology**: Presents the relevant data for grid design, case study description and provides the experimental method and design concepts for the analyses in this dissertation such as the load flow analyses and BESS modelling with peak shaving used in Simulink.

Chapter 4 - **Results and Discussion**: Provides the results from the simulations and the voltage alleviation is summarised and discussed.

Chapter 5 - **Conclusion**: Gives a summary of the project work, main results and remarks on the work conducted.

Chapter 6 - **Recommendations** and **Suggestions**: Recommendations to improve the current work and suggestions for further work containing added parameters.

2. Background theory

2.1 The Norwegian power system and infrastructure

The Norwegian power network facilitates the movement of electricity from generation sources to end users. This network is structured into three distinct tiers: the central transmission grid, the regional distribution grid, and the local distribution grid. Serving as the main arteries of the power infrastructure, the transmission grid, often referred to as the central grid, bridges major power generating regions with high-consumption zones across the country. The governing body for this grid segment is the transmission system operator (TSO), Statnett [6].

As per European Union regulations, both the regional and local grids fall under the distribution category. These sections deliver power to end-users and are managed by various distribution system operators (DSOs) [6]. Given the substantial capital requirements for grid development, constructing multiple grids in a single location for competitive purposes is not cost-effective. As such, the power grid inherently operates as a monopoly, preventing competitive ventures.

In Norway, the transmission grid voltage range is between 400kV – 300kV, the regional distribution grid voltage range is between 132kV – 33kV and the local distribution grid voltage range is between 22kV – 0.230kV [6]. The local distribution grid, linking end-users to the network, encompasses both high and low voltage sections. In this context, voltages exceeding 1kV are categorized as high voltage and the low voltage is either 230V or 400V. While more substantial power generation facilities interface with the regional or transmission grids, the distribution grid often accommodates smaller commercial buildings and residential homes.

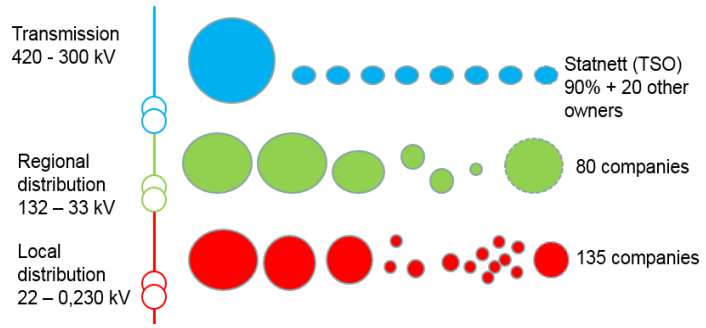

Figure 2.0 Structure of the Norwegian power system infrastructure

Taken from [6]

2.1.1 The Regulation on the delivery of quality (FoL)

It is important to highlight the regulations that govern delivery quality in the grid, this regulation is called the Forskrift om leveringskvalitet i kraftsystemet (FoL) which is translated by the author to[1]; The regulation on delivery quality in the power system. The main points of the regulation **related to voltage quality** are listed below which are also translated to English by the author to [2]:

§ 3-2 Voltage frequency

The System Responsible party shall ensure that deviations in voltage frequency and timing are normally kept within the provisions of the Nordic system operation agreement.

The System Responsible party shall, in areas that are temporarily without a physical connection to adjacent transmission networks, ensure that the voltage frequency is normally kept within 50 Hz ± 2% [7].

§3-3 Slow variations in the effective value of the voltage

The grid company shall ensure that slow variations in the effective value of the voltage are within a range of ± 10% of the nominal voltage, measured as an average over one minute, at the connection point in the low voltage network [7,8].

§ 3-4. Transient over voltages, transient under voltages, and voltage changes

The Energy Regulatory Authority can instruct those covered by this regulation to implement measures to reduce the scope or consequences of transient over voltages and under voltage.

The grid company shall ensure that voltage changes during transient over voltages, transient under voltages, and voltage changes do not exceed the following limit values at the connection point with the respective nominal voltage level, U_n, for the respective time interval [7].

Table 2.0 Transient overvoltage and under voltages allowed.

Taken from [7]

Transient overvoltages, Transient undervoltages and Voltage spike	Maximum number allowed per concurrent 24-hour period	
	0.23 kV ≤ V_N ≤ 35 kV	35kV < V_N
$\mathbf{\Delta V_{stationary}}$ ≥ 3 %	24	12
$\mathbf{\Delta V_{max}}$ ≥ 3 %	24	12

§ 3-6 Voltage Imbalance

The grid company shall ensure that the degree of voltage unbalance does not exceed 2% at the connection point, measured as an average over ten minutes.[7]

[1,2] Translated by the author.

2.1.2 The local distribution grid

Grid operators in Norway have historically ensured that the distribution system could accommodate peak anticipated loads, ensuring voltages remained above specified minimums during substantial loads and preventing excessive current from thermally stressing the grid infrastructure like cables and transformers. To achieve this balance, substations were calibrated to maintain non-excessive voltages during low loads, and the infrastructure was also designed to manage voltage dips within permissible levels. Norway's electrical generation is dominated by hydroelectric energy which accounts for 92% of electricity generation [9] and as such, the high voltage grid had to accommodate large power injection. With the advent of PV systems installed at residential houses and with consumers sending power back to the local distribution grid, transformers are now configurated to operate at voltage around 240-245 V to allow for a good margin for voltage drop throughout the network. Without reconfiguration, these transformers would have had have limited capacity to accommodate additional voltage rise due to solar power injection.

The transformer's apparent power rating is determined by the current it can manage at its specified voltage. This is typically quantified in VA and is derived from the following equation (2.1) [10]

$$S_n = \sqrt{3} \cdot V_n \cdot I_n \quad , \tag{2.1}$$

where S is the nominal power in kVA, kV is the nominal voltage, and I is the nominal current represented as A [10].

The apparent power is one of the main infrastructures that influences how much load a grid can maintain. However, the transformer load should not exceed 120% at maximum load [10].

2.1.3 Earthing systems in the local distribution grid

There are two types of earthing systems used in the low voltage distribution grid in Norway, they are 230 V IT (Insulated Terra) and 400 V TN (Terra Neutral). Even though many countries use TN earthing systems, the Norwegian power system is dominated by IT earthing systems, with between 70-80% of total installation [11]. In this dissertation the case study of the local distribution low voltage grid is a 230 V IT system.

IT systems:

A significant portion of the Norwegian distribution system operates on a unique 230 V IT grid, a setup distinct to Norway within Europe. Most other European nations predominantly rely on various adaptations of the 230/400 V TN network. This distinction poses complexities, especially concerning electrical devices, as many products designed for the TN network require modifications to be compatible in the Norwegian context [12].

The Insulated Terra system (IT), represented by "I", signifies that the power supply either lacks a functional ground or has a high impedance grounding. The "T" indicates that the devices on the load side are grounded [13].

Advantages of IT systems:

- **High Reliability:** Ensures a dependable power source, particularly over shorter distances.
- **Optimal Security:** Minimizes risks of outages or disturbances.
- **Continuity:** Ideal for environments demanding uninterrupted power supply such as electric power to factories, hospital operating rooms, and other critical infrastructure [13]

Disadvantages of IT systems**:**

- **Distributed Capacitance:** Over extended distances, the capacitance between the power supply line and the earth becomes significant.
- **Protection Device Inefficiency:** In case of a short-circuit fault or load leakage that electrifies the device casing, the leakage current might route through the earth without triggering the protection device. This can cause be a potential source of fires
- **Reduced voltage**: A limitation of the IT system is that it has a reduced line voltage compared to TN-systems, leading to increased currents and elevated losses [13].

TN systems:

The TN system, characterized by its neutral-grounded three-phase grid configuration, ensures that the exposed conductive components of all electrical apparatus are grounded at a singular point in the power supply, typically the neutral point of the distribution system [13]. This design aids in quickly forming a closed loop during short-circuit scenarios, producing a significant short-circuit current that prompts protective devices to act swiftly. The TN system's distinction between the neutral (N) line and protective Earth (PE) line enhances safety, though it's pivotal to avoid commingling the two to preserve the system's advantages. There are three different variations of TN systems, they are; TN-C systems, TN-S systems, and TN-C-S systems [13].

Advantages of TN systems**:**

1. **Higher line voltage:** Because the TN system operates at 400 V, it can tolerate more variations in voltages. Additionally, the magnitude of variations is lower than that experienced in IT systems due to the higher peak line voltage of the system.
2. **Rapid Fault Detection:** Upon short-circuiting, the TN system quickly forms a metallic single-phase short circuit, producing a large current that ensures protective devices act promptly.
3. **Isolated Neutral and PE lines:** The three-phase five-wire system in the TN setup ensures that the neutral (N) and protective Earth (PE) lines are separate, boosting safety.

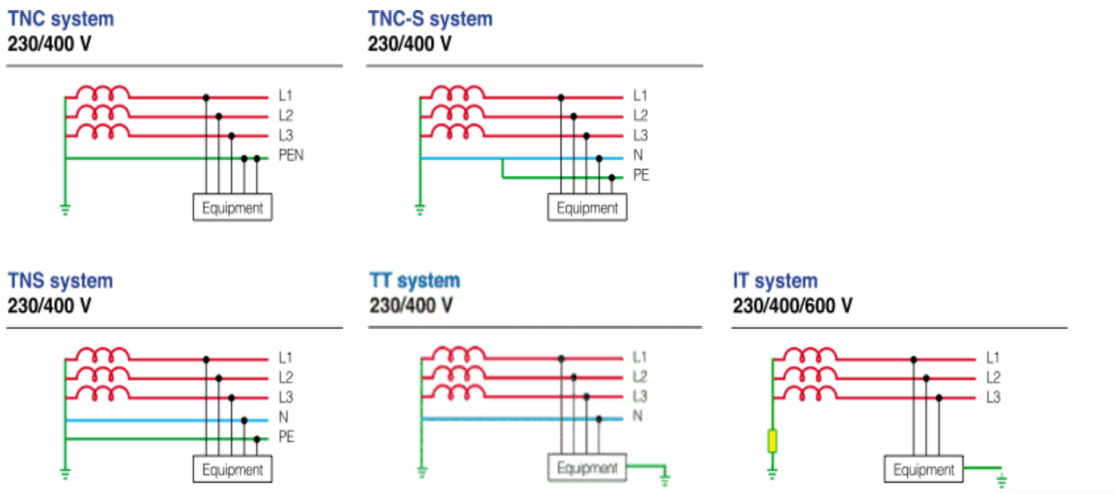

Figure 1.1 Configurations of TT and TN systems

Taken from [13]

2.1.4 Reverse flow and grid strength

When the PV system generates more energy than what the consumer utilizes, the surplus energy is sent back to the grid, leading to reversed power flow. As depicted in Fig. 2.2, when the power production (PG + QG) surpasses the power consumption (P_L + Q_L), the current I_1 moves from the customer towards the grid. The subsequent voltage drop across the cable's impedance (incorporating resistance R and reactance X) transitions from the customer's end V_2 towards the substation V_1, resulting in a voltage elevation. This voltage magnitude must remain within the stipulated range as directed by the regulation on the delivery quality in the power system (FoL) [8]. This criterion allows slow voltage variations of ±10%, measured in one-minute intervals [8]. This can be represented by the following expression

$$0.9 \cdot V_n \leq V \leq 1.1 \cdot V_n \ , \tag{2.2}$$

where U_n representing the nominal voltage, we can deduce that the acceptable voltage range for customers in a 230 V IT system lies between 207 V and 253 V. Furthermore, for a 400 V TN system, the permissible range is from 360 V up to 440 V.

As stated earlier, PV surplus production will lead to an increase in voltage and can be calculated using equation (2.3)

$$\Delta V = \frac{1}{V_2} \cdot [(P \cdot R - Q \cdot X) + I \cdot (P \cdot X + Q \cdot R)] \ , \tag{2.3}$$

where ΔV represents the voltage variation, either a decrease or an increase, in (V)from one busbar to another. The voltage at the secondary busbar is denoted by V_2 in (V). P and Q, measured in (W) and (var) respectively, indicates the active and reactive power, whether consumed or produced, at this second busbar. The resistive and inductive components of the impedance in the

connecting cable between the busbars are represented by R and X, and the current increases as voltage increased the as shown in equation in (2.3). Equation (2.3) can be further simplified below modified to [14]

$$\Delta V \approx \frac{(P \cdot R + Q \cdot X)}{V} \tag{2.4}$$

This voltage increase is influenced by the amount of power fed into the grid and the grid's robustness, with the latter often limited by the short circuit current. High PV production, when combined with high impedance, might push voltage levels beyond the stipulated boundaries [15]. Additionally, if the generated power surpasses a component's thermal capacity, such as a cable or transformer, it can lead to overheating or trigger protective mechanisms to activate [15,16].

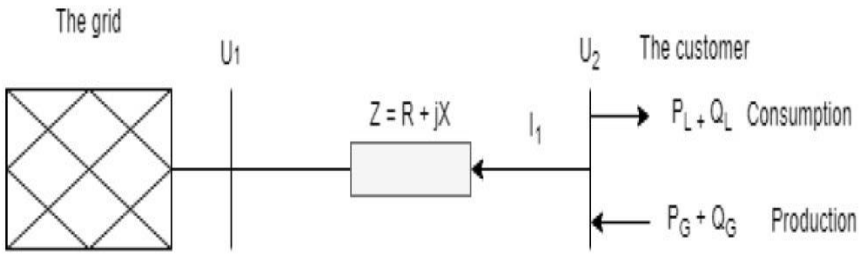

Figure 2.2 Impact on the grid due to reverse flow of production

Adapted from [15]

For the grid to operate under voltage rise from DERs, the grid strength must be adequate to handle both high PV production with low consumer load in the summer and low PV production with maximum PV load during the winter.

The robustness of a grid pertains to its capacity to manage alterations in power transfer. Grids characterized with a low short-circuit ratio or a high R/X ratio are termed weak and have limited power transfer capability [17]. Such grids have significant impedance with diminished reactance (X), implying that the line and cable resistance is substantially large relative to the reactance. Alternatively, these weak grids can experience considerable voltage reductions and energy losses while subjected to high load demand.

The ratio between reactance and resistance, denoted as the R/X ratio, serves as a standard metric for defining the inherent qualities of cables and lines. Low voltage grids typically have higher R/X ratios in comparison to high voltage grids. Furthermore, underground cables generally have a reduced R/X ratio compared to overhead lines [18]. Another consideration is the assumption that the PV system doesn't adjust for any reactive power. Given that the relationship between resistance and reactance (R/X ratio) is predominantly influenced by total resistance (impedance and line resistance), the reactive component becomes less significant and can be deemed negligible. However, the R/X ratio balance shift more towards being reactance-dominant when the lines/cables are in a closer proximity to the substations.

Table 2.1 To calculate voltage drop in low voltage systems.

Taken from [15]

Grid	**IT system**	**TN system**
Single phase	$\Delta V = \frac{P_R}{I_{SC2}}$	$\Delta V = \frac{\sqrt{3} \cdot P_R}{I_{SC2}}$
Three phase	$\Delta V = \frac{P_R}{2 \cdot I_{SC2}}$	$\Delta V = \frac{\sqrt{3} \cdot P_R}{\sqrt{3} \cdot 2 \cdot I_{SC2}}$

2.2 Measures to avoid overvoltage.

2.2.1 Grid infrastructure improvements

Enhancements to the grid to bolster its resilience can be executed through increasing the cross-sectional area of the overhead lines or cables [19]. This increases transmission capacity but also enhances short circuit currents due to reduced resistance thereby decreasing the R/X ratio as well. Another grid enhancement is constructing additional substations and increasing the capacity of the transformer(s) nearest to the end-users is another viable approach, albeit cost-intensive [19]. These two methods are commonly referred to as grid re-enforcement.

2.2.2 Transformers

The On-Load Tap Changer (OLTC) facilitates voltage adjustments at the lower level of a transformer without necessitating system de-energization. This approach proves efficacious when all feeders connected to the transformer exhibit analogous load profiles [20]. Given that a secondary substation typically interfaces with multiple feeders, the control mechanism must simultaneously modify the set point across all feeders, rather than exclusively focusing on the most critical feeder. Such simultaneous adjustments might result in over voltages in certain network segments while concurrently causing undervoltage in others, rendering the method suboptimal in certain situations. Another inherent drawback is the stress exerted on the OLTC, potentially diminishing its operational lifespan [20].

Fundamentally, OLTCs play a pivotal role in voltage modulation. They utilize a dynamic connection point, termed a tap, positioned along a transformer winding. This tap enables the selection of specific turn numbers, with designated positions known as tap positions, symbolized by “ƈ’’. Through altering the tap position, OLTCs modulate the voltage ratio, transitioning the secondary voltage in relation to the primary. The tap ratio is denoted as “a’’ and a =1 when ƈ=0 [21].

2.2.3 Droop control

The droop control strategy is predominantly adopted in PV power frameworks to facilitate automated load distribution among diverse distributed PV configurations, while enhancing the functional scope of the specified inverter(s) [24]. This works by measuring the nominal active power (P_{nom}) and reactive power (Q) for the nominal frequency (F_{nom}) and the nominal voltage (V_{nom}) to be drooped thereby employing the same characteristics of a synchronous generator [24].

For controlling the point of common coupling (PCC) voltage magnitude, a (Q-V) droop control strategy is implemented meanwhile for controlling the frequency of the system then a (P-f) droop control is implemented [24].

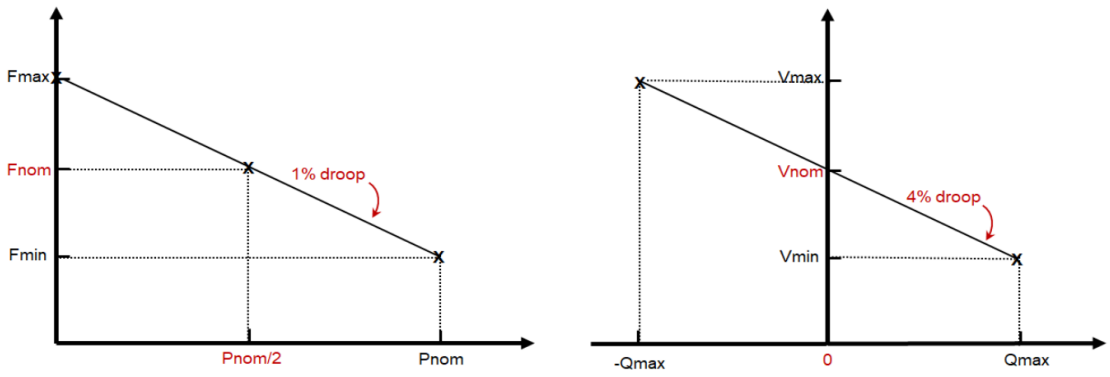

Figure 2.3 PV inverter droop control strategy

Taken from [25]

2.2.4 Active power curtailment

Local distribution grids are being subjected to a rise in the integration of distributed photovoltaic (PV) systems due to their growing cost-effectiveness. Such heightened levels of integration can influence distribution circuits in multiple manners, with one of the most notable impacts being on voltage stability.

Active power curtailment seeks to avert voltage variations by moderating the active power production of a solar PV system via the inverter [26]. This curtailment objective is to stabilize the PV power output by constraining power production, thereby mitigating potential voltage shifts [26].

2.2.5 Reactive power control

During periods where PV's maximum generation aligns with minimal load scenarios, the voltage at point of common coupling (PCC) surges significantly. This timeframe is crucial for voltage elevation, and proper control is essential to revert the voltage to its required operational range. Reactive power management involves the PV inverters injecting or absorbing reactive power in response to voltage increases or decreases at PCC [27]. Owing to its scalability, efficiency, adaptability, and dependability, reactive power control is an effective strategy for voltage regulation [27]. Furthermore, its implementation can be adjusted based on desired precision and budget constraints.

2.2.6 Upgrading of IT systems to TN systems.

As mentioned earlier in 2.1.3, a significant portion of the Norway’s local distribution gird network is based on the 230 V IT system. In relation to voltage tolerances and stability this type of system is not as resilient as the TN (and TN subsystems) due to its reduced line voltage. Upgrading to the TN system which operates at 400 V will tolerate voltage fluctuations significantly better than IT grid systems and as such reduce occurrences of voltage rise above the specified limit. However, due to the significant cost of upgrade upgrading the entire Norwegian grid may not be economically feasible but instead planned upgrades and newly connected areas should utilize the TN system [28].

2.2 Battery Energy Storage system (BESS)

The Norwegian grid is currently experiencing significant change due to DERs such as PV systems increasing in number. Also, at the same time, the grid is getting older as a large portion of the grid was built between 1950 and 1980s which was developed under traditional conditions [29]. As mentioned in chapter 1.2, additional energy fed into the grid by residential PV installations can cause voltage rise leading to grid instability. By combining PV installations with BESS, the extra energy can be stored and used at a later period when additional energy is needed thereby causing a reduction in voltage rise.

There are three main components of the battery energy storage system (BESS); 1) the battery, 2) inverter and or power conversion system and the 3) battery management system (BMS) that controls the functionality of battery as represented in fig. 2.4.

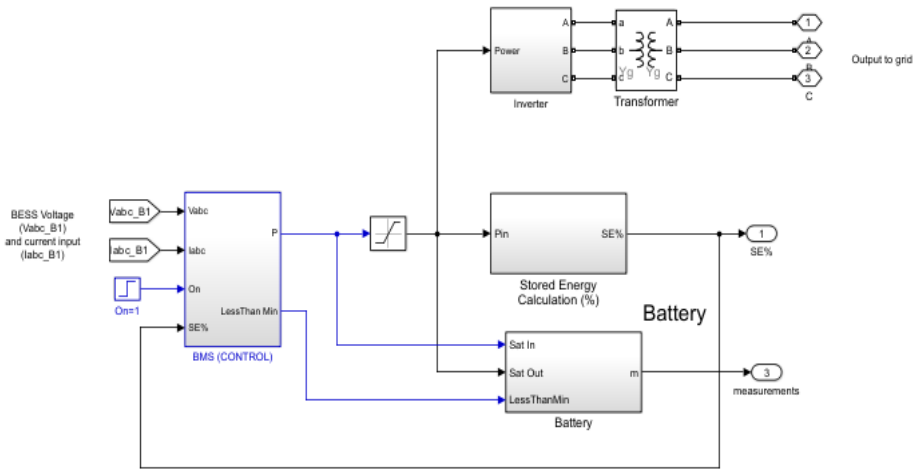

Figure 2.4 Overview of a BESS in Simulink connected to the grid.

2.3.1 BESS characteristics

Batteries can aid in minimizing distribution system inefficiencies, eliminate current obstacles for incorporating renewable distributed energy sources, and assist in maintaining voltage and frequency stability. As stated in reference [31], due to their modular nature, flexibility and available in diverse sizes, a battery energy storage system is well suited for grid management. BESSs can be segmented into mobile and stationary categories. The stationary types can be further classified into utility-scale front of the meter (FTM) or behind-the-meter (BTM) applications. Various battery technologies present in the market differ significantly in their features, influenced by their chemical makeup. However currently, Lithium Ion (Li-ion) batteries account for 78% of BESS in operation [30] and as such this dissertation will cover only stationary, utility FTM Li-ion battery energy storage systems.

Lithium-ion batteries are well suited for grid storage applications because they boast a superior cycle life and elevated power density relative to other battery varieties [31,32]. Additionally, they possess a rapid charge and discharge capability and round-trip efficiencies between 80%-90% whilst having minimal self-discharge risks [31,32].

However, there exists some negative drawbacks such as Lithium-ion batteries being affected by heat, high capital cost and like most batteries, the life cycle is dependent on the operation of use [32].

2.3.2 Battery energy storage

One of the major obstacles preventing BESS integration is the capital cost. While still relatively expensive, one positive trend shown over the past years is the steady decline of the price. In a 2023 report referenced from [33], the cost of Li-ion BESS can reduce by as much as 47% in the next seven (7) years.

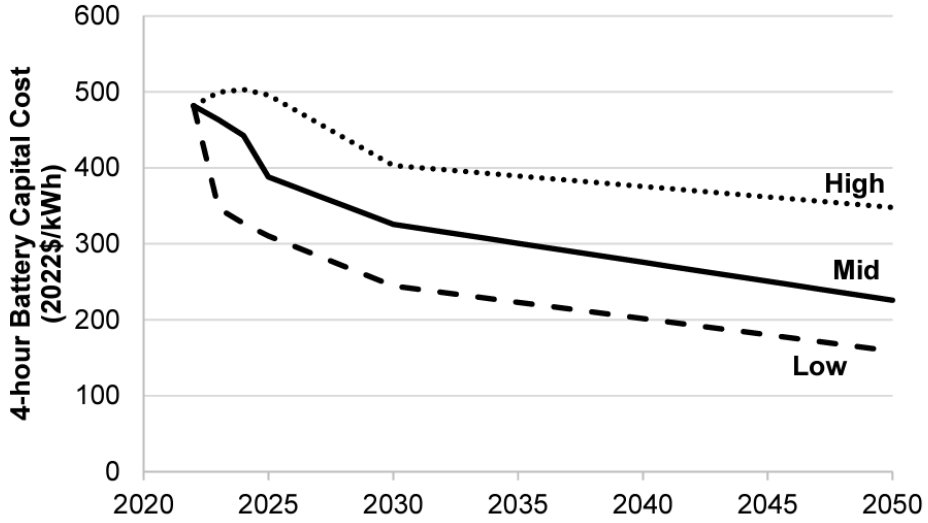

Figure 2.5 NREL 2022 Li-ion cost trend

Taken from [33]

BESS at the utility scale in the distribution grid brings into play several services that can be provided to maintain grid stability. These services inadvertently can facilitate further development of DERs such as more PV systems and other small-scale DERs that can be installed in the low voltage grid. A summary of some of the other services that can be provides by batteries to the grid are shown in fig. 2.6 provided by the Rocky Mountain Institute [37].

Within its capacity constraints, a BESS can offer both active and reactive power, making it valuable for controlling voltage and frequency in power systems [35,36]. In LV networks, ensuring adequate active power becomes paramount for the battery as it guarantees regulation of both frequency and voltage. While BESSs used for frequency regulation might not demand extensive energy capacity, those intended for prolonged voltage regulation may demand more energy capacity [34,35,36]. Due to the extra capacity needed to effectively conduct voltage regulation, a battery management system strategy such as peak shaving that ensures flexibility and adaptability can be advantageous to offset this added expenditure.

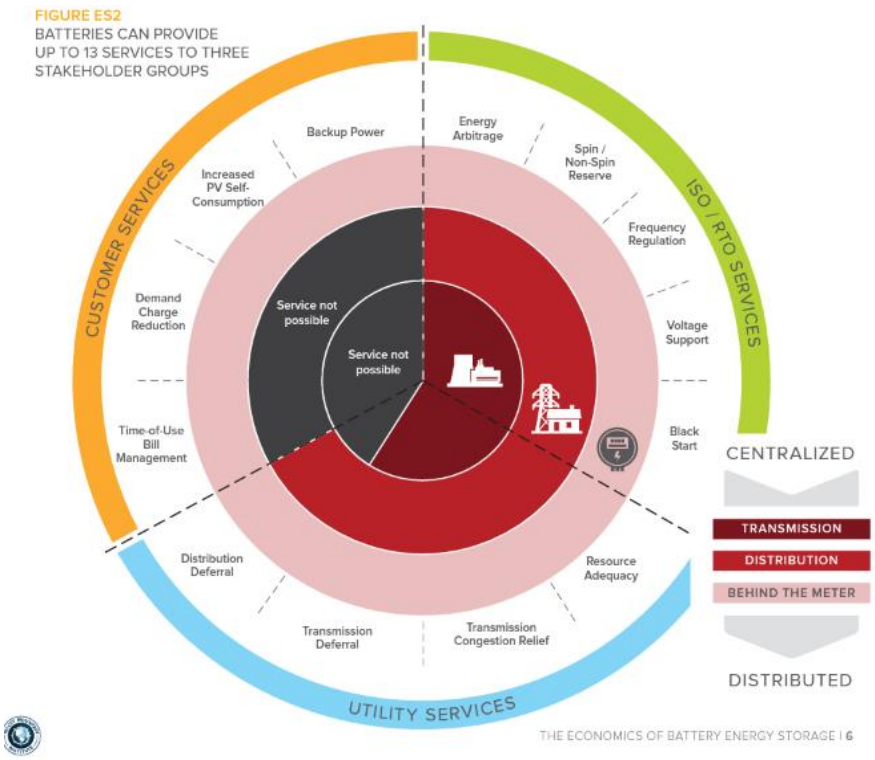

Figure 2.6 Services provided by battery energy storage systems.

Taken from [37]

2.3.3 Peak Shaving

One growing application for the alleviation of high PV production in low voltage grids is the use of peak shaving. This is applicable due to the general nature of peak demand being mostly during the late afternoon and night meanwhile the peak PV production occurs typically during mid-day creating a mismatch for optimal use of energy.

For the strategy to be effective providing voltage control, the use of a control algorithm to maximize or minimize functions are used.

There are many algorithms that can address this including many versions of categorical variable decision tree algorithms (CVDTA) which reduces peak demand where the addition of capacity is not appropriate [38].

Another peak shaving strategy to mention is the ultimate peak load shaving (UPLS) which is noted to be applicable for any condition and load whilst controlling the charging and discharging logic [39].

Peak Demand control (PDC) algorithms is another frequently used method due its simplicity and practicality. These algorithms operate by analysing real time or historic consumption data thereby contributing to a more evenly spread energy consumption. This also ensures that the BESS reduces the peak loads on grid and maximises the use of the DER [40].

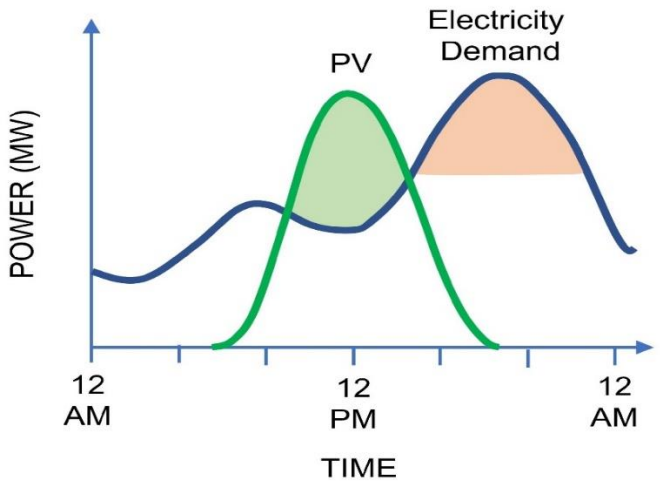

Figure 2.7 Peak shaving operation with PV production

Taken from [41]

3. Methodology

3.1 Data basis

For this dissertation a load profile for an area (POS) in Norway for the year 2022, consisting of ten (10) consumers in a low voltage 230 V IT grid were given by a local DSO as seen in Fig.3.0.

For simplicity of simulation, the load data from 18th April 2022 was taken and used in the simulation of the model and further analysed. The rationale behind using this date as the case study was due to the very low load demands experienced on that day coupled with large PV production. The data provided is active power consumption and all reactive power information are assumed by the author in-order for the simulations to function.

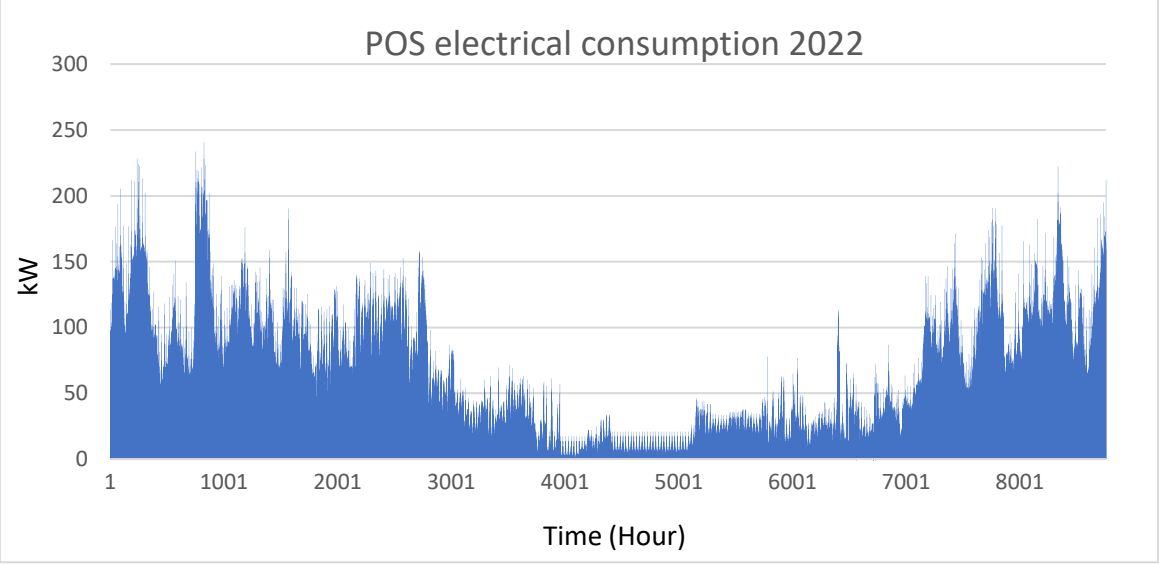

Figure 3.0 Load demand in 2022

Table 3.0 Load data on 18th April

Aggregated energy consumption for 18th April	1.09 MWh / 1094 kWh
Aggregated maximum load demand	106 kW
Aggregated minimum load demand	20 kW
Lowest load demand period	1100 hrs – 1600 hrs
Highest load demand period	1730 hrs – 2100 hrs

These consumers do not have PV systems but for this dissertation PV systems are synthetically added to the consumers with the purpose of generating surplus PV production that is fed back into the grid. In this case study, the PV systems will have a maximum power production capacity of 16.3 kWp, with shading inefficiencies assumed to be negligible and all roof orientations are assumed to be the same. The importance of this is to mimic a worst-case scenario of high PV production being generated by at all the houses. The total area of PV panels equated to 781.2 m^2 and this is used as an input in Simulink to calculate PV production given the irradiance and air temperature data. The calculation of area required is shown in appendix A.

The irradiance and air temperature values used were from 2020 and was taken from the SARAH-2 solar radiation data referenced from [42] as the author could not source more recent data readily available. PVGIS-SARAHs uses the images of the METEOSAT geostationary satellites covering Europe, Africa, and Asia (±65° longitude and ±65° latitude) [43]. From this source, the hourly global irradiance (kWh/m2) and air temperature (C°), on an optimally inclined surface, for latitude 58°23'59"N was used [42]. Longitude values are omitted to maintain the anonymity of the location.

3.2 Grid composition

The grid information was provided by the DSO along with line specifications, transformer data and the general layout of the grid. The layout and line specifications was also used in [44] but aim of that study focused on techno economics of a BESS and not it's use in alleviating voltage rise due to high PV penetration in the grid.

The layout of the grid is divided into two radials with a total of 10 consumers. Three (3) of the consumers are located on radial A1 (on the left) and seven (7) consumers are located on radial A2 (on the right) as illustrated in Fig. 3.1

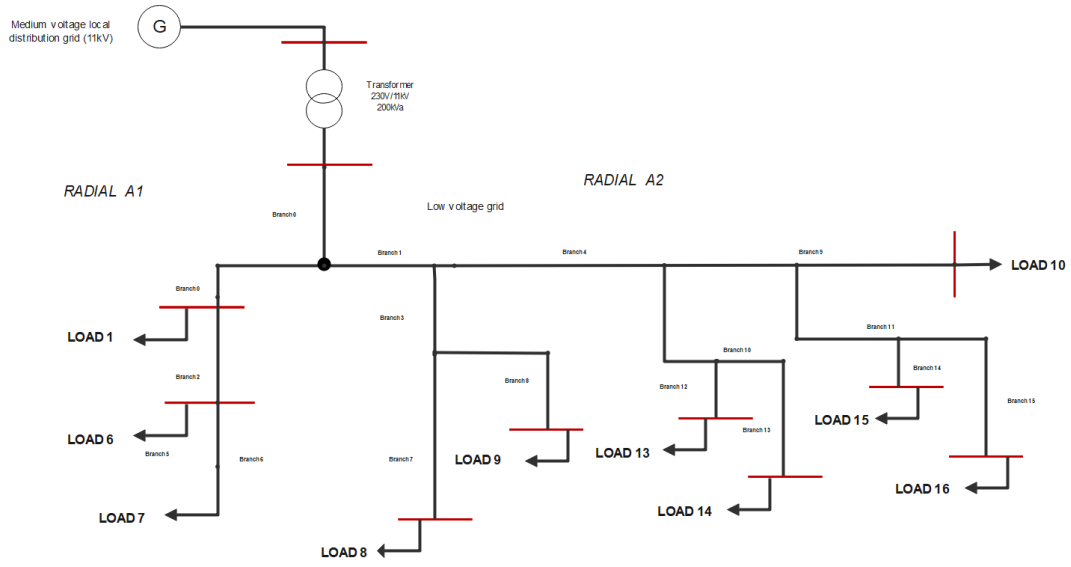

Figure 3.1 Topology of POS Grid

The line data of the POS grid is predominantly overhead lines using aluminium (AL) and copper (Cu) cables. The lines capacitive reactance and resistance information was given by the DSO but the impedances and reactive inductances were calculated by the author.

Table 3.1 Line specifications

Line	R (Ω/km)	X (Ω/km)	R/X ratio	X/R ratio
Cu3 x 16	1.11	0.294	3.77	0.26
EX3 x 95 AL	0.308	0.075	4.10	0.26
EX3 x 50 AL	1.178	0.079	14.91	0.067
EX3 x 25 AL	1.2	0.082	14.63	0.068

The transformer that feeds the low voltage distribution grid has an apparent power of 200kVA which supplies a secondary line voltage of 230V with an assumed power factor as 1.

The apparent power is found via the equation [10];

$$S_n = \sqrt{3} \cdot V_n \cdot I_n, \quad (3.1)$$

Where;

S_n = Nominal apparent power

V_n = Nominal voltage (V)

I_n = Nominal current in amperes (A)

3.3 Load flow simulation of the case study

An overview of the methodology used for the simulation is presented in this section. In the previous sections (3.1 and 3.2), the POS grid composition, line and load profiles were presented as to provide the fundamental information needed to design the POS grid in Simulink and the implementation of load flow analyses with and without 16.3 kW PV systems.

Per-Unit (pu) is commonly used for electrical calculations especially grid applications as to improve the ease of communication to a wider audience. In this dissertation the base voltage that will be used is 230V and is equated to a per unit value of 1.

Before the simulation of the load flow analyses some parameters need to be calculated and included in the model. As stated in section 3.2, the reactive inductance and base impedance values are calculated by the author and this was done using equation (3.2) and equation (3.3),

$$\text{Base impendence } (\mathrm{Z_{base}}) \ : \ \mathrm{Z_{base}} = \frac{\mathrm{V_{base}^2}}{\mathrm{S_{base}}} \tag{3.2}$$

$$\text{Reactive inductance } (\mathrm{L}) \quad : \mathrm{L} = \frac{\mathrm{X} \cdot \mathrm{Z_{base}}}{2 \cdot \pi \cdot 50} \tag{3.3}$$

An example of one calculation is given in appendix B.

Z_{base} was calculated and the table (3.2) below was developed.

Table 3.2 Base system values

Parameter	Base value
$\mathbf{S_{base}}$	1 kVA
$\mathbf{V_{base}}$	230 V
$\mathbf{Z_{base}}$	52.9 Ω

Table 3.3 Summary of Line data

Bus/Consumer	Length (m)	Line type	R(Ω)	X (Ω)	L (H)	R/X ratio	Z(Ω) actual	Zbase	Base voltage	S base (va)
0	370	EX3x95	0.11396	0.02775	4.67E-03	4.11E+00	6.03E+00	5.29E+01	230	1.00E+03
1	100	EX3x50	0.1178	0.0079	1.33E-03	1.49E+01	6.23E+00	5.29E+01	230	1.00E+03
2	675	EX3x95	0.2079	0.050625	8.52E-03	4.11E+00	1.10E+01	5.29E+01	230	1.00E+03
3	40	EX3x50	0.04712	0.00316	5.32E-04	1.49E+01	2.49E+00	5.29E+01	230	1.00E+03
4	50	EX3x25	0.06	0.0041	6.90E-04	1.46E+01	3.17E+00	5.29E+01	230	1.00E+03
5	35	EX3x50	0.04123	0.002765	4.66E-04	1.49E+01	2.18E+00	5.29E+01	230	1.00E+03
6	35	Cu3x16	0.03885	0.01029	1.73E-03	3.78E+00	2.06E+00	5.29E+01	230	1.00E+03
7	20	Cu3x16	0.0222	0.06802721	1.15E-02	3.26E-01	1.17E+00	5.29E+01	230	1.00E+03
8	75	EX3x25	0.09	0.00615	1.04E-03	1.46E+01	4.76E+00	5.29E+01	230	1.00E+03
9	60	EX3x25	0.072	0.00492	8.28E-04	1.46E+01	3.81E+00	5.29E+01	230	1.00E+03
10	25	EX3x25	0.03	0.00205	3.45E-04	1.46E+01	1.59E+00	5.29E+01	230	1.00E+03
11	50	EX3x25	0.06	0.0041	6.90E-04	1.46E+01	3.17E+00	5.29E+01	230	1.00E+03
12	50	EX3x50	0.0589	0.00395	6.65E-04	1.49E+01	3.12E+00	5.29E+01	230	1.00E+03
13	40	EX3x25	0.048	0.00328	5.52E-04	1.46E+01	2.54E+00	5.29E+01	230	1.00E+03
14	35	EX3x25	0.042	0.00287	4.83E-04	1.46E+01	2.22E+00	5.29E+01	230	1.00E+03
15	25	EX3x25	0.03	0.00205	3.45E-04	1.46E+01	1.59E+00	5.29E+01	230	1.00E+03
16	60	EX3x25	0.072	0.00492	8.28E-04	1.46E+01	3.81E+00	5.29E+01	230	1.00E+03

3.4 Grid development for load flow analyses

3.4.1 Grid design and load flow results

The load flow analyses are done in a series of steps as detailed by the author below. Also, they were created using a variable-step automatic solver selection. This was chosen as this solver can be adaptive to the various types of datasets present in the simulations.

Step one involved the representation of the grid with data and numerical information for line, branches, buses, and this information was taken from Table 3.3. The inspiration of the grid layout is taken from the topology shown in Fig. 3.1. The grid development and design were original work done by the author, but the residential load blocks were created by Jonathan Le Sage [45] and its numerical inputs were altered by the author.

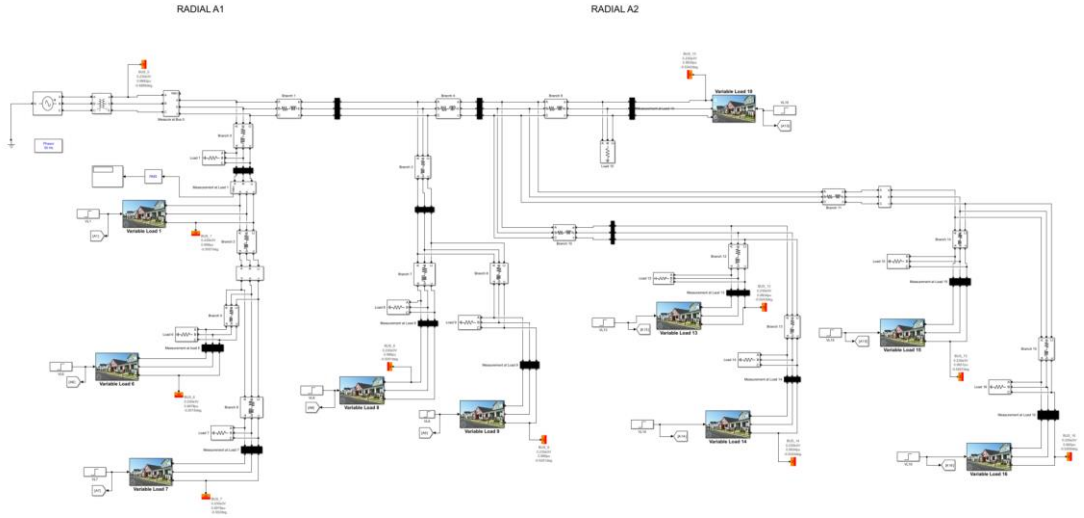

Figure 3.2 POS grid designed in Simulink without PV systems.

The initial loads during this simulation were all set at different times and different values as to replicate an unbalanced load demand which is also representative of real-world scenarios as shown in appendix C. The primary goal of this is to record the voltage drop across the grid to ascertain the resilience of the grid. The voltage drop variations are illustrated in Fig. 3.4 and Fig 3.5.

Step two involves a similar method as step one with the only alteration being the introduction of the PV systems at the loads. All PV systems at the start of the simulation will all be generating 2 kW. At the 5 second point, a step change is activated to achieve a maximum power of 16.3 kW for all consumers which is justified by the limitations stated in chapter 1.5. Similar to step one, the grid development and design was original work done by the author, but the residential load and PV blocks were created by Jonathan Le Sage [46] with modifications and the numerical input to all Simulink blocks and buses done by the author.

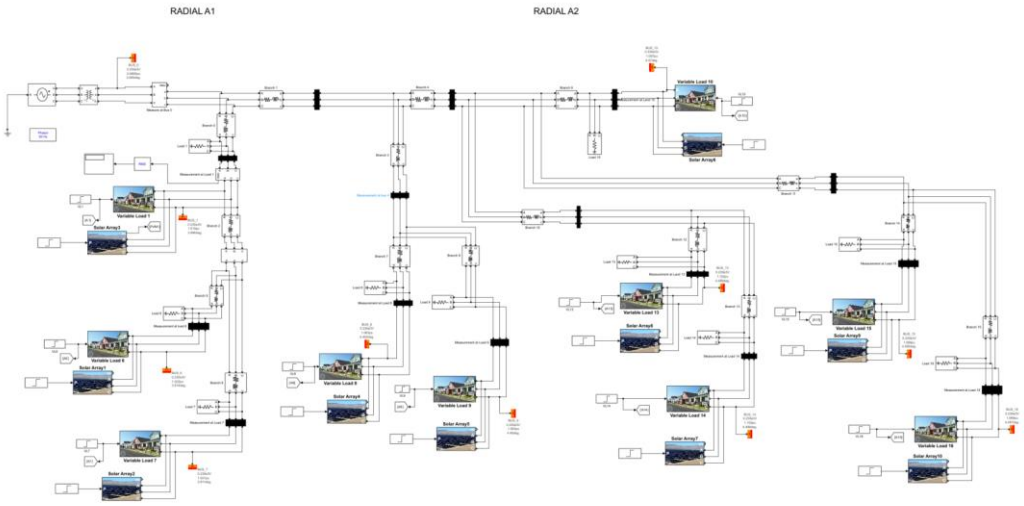

Figure 3.3 POS grid designed in Simulink with PV systems.

Step one provides the baseline voltage variations and voltage drop across the grid at the different consumers with unbalanced loads and at different distances from the transformer. Meanwhile, step two provides the voltage variations and voltage rise across the grid when PV-systems are added to all consumers with unbalanced loads as seen in Fig. 3.6. A summary of the load flow analysis using Simulink's load flow analyser is shown in appendix D.

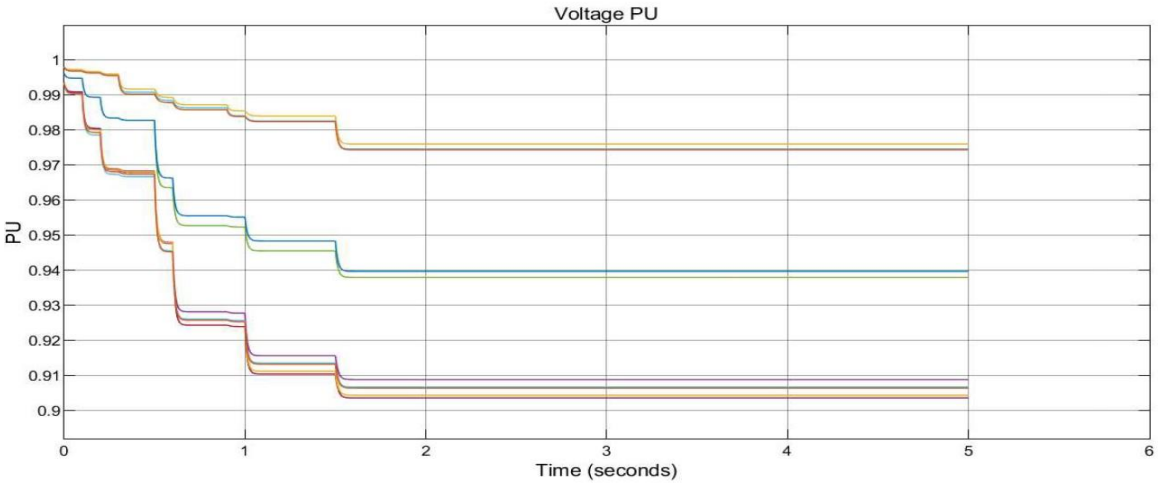

Figure 3.4 Voltages in pu for all consumers without PV systems

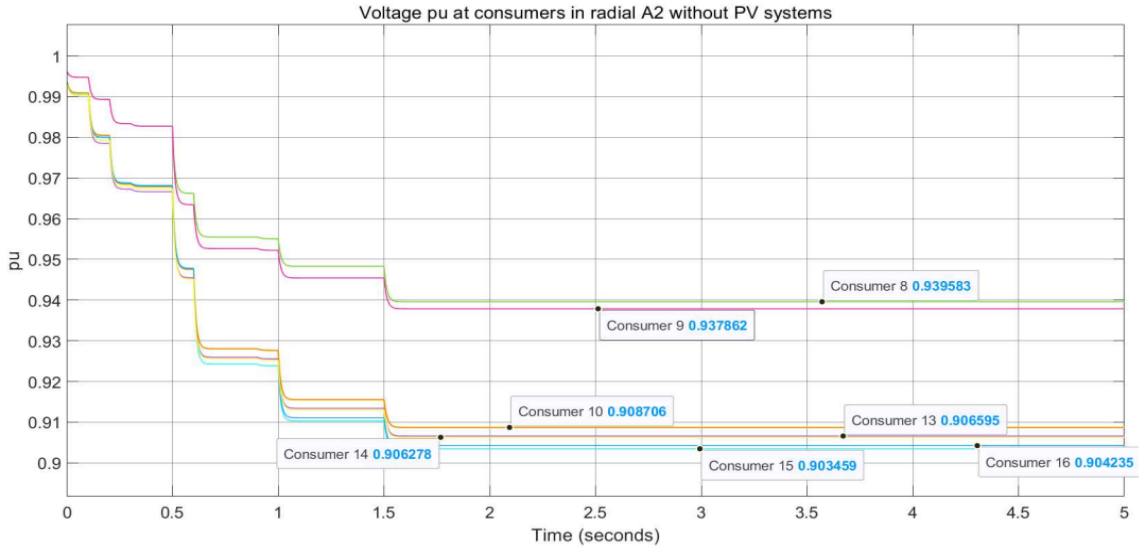

Figure 3.5 Voltages in pu for consumers in radial A2 without PV systems

The consumers in radial A1 all had voltages above 0.97pu without PV installations and voltages below 1.05 pu with PV installations which suggests that they are not susceptible to larges voltage variations due to the transfer of energy in the grid. As a result, more focus will be placed on radial A2. The voltage drop variations serves as a rational for further investigations and simulations using the load profile data from 18th April in this dissertation.

Appendix D contains a list of voltages of all consumers with and without PV systems.

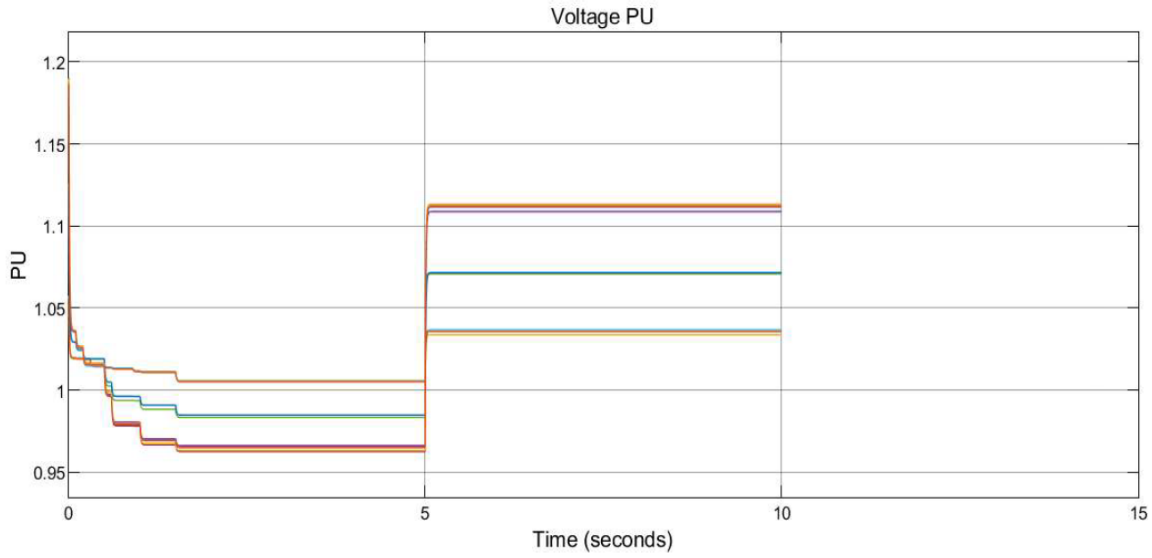

Figure 3.6 Voltages in pu for all consumers in the grid with pv systems.

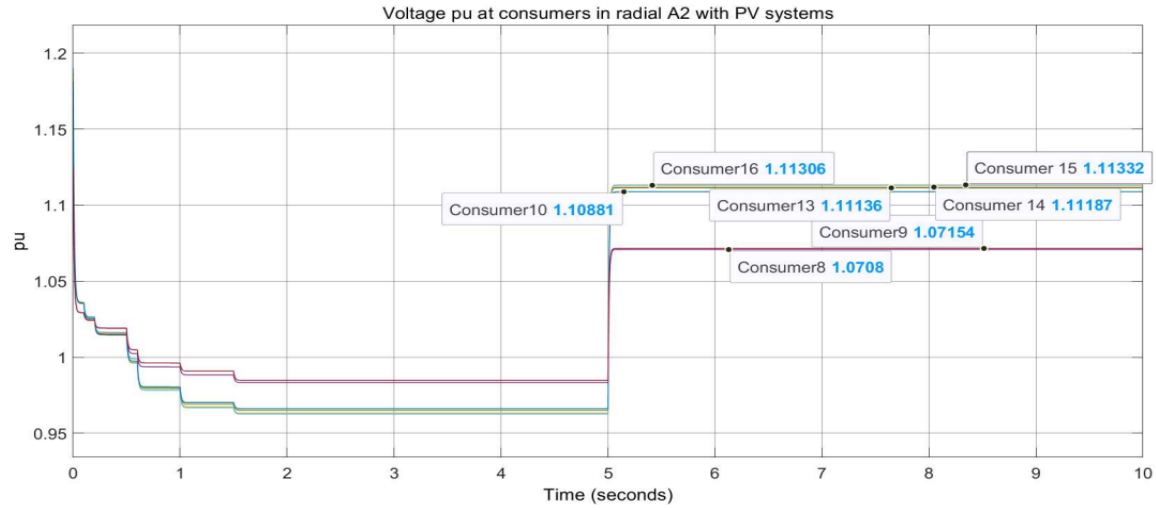

Figure 3.7 Voltages in pu for all consumers in radial A2 with PV systems.

As seen in figures 3.4 – 3.7 consumers in radial A2 are more susceptible to voltage drop when energy is transferred from the transformer to meet the load demand and voltage rise when energy is transferred from the PV systems back to the grid. Additionally, consumers 16,15,13,14 and 10 experienced voltage elevations above 1.10 pu when the PV systems were in operation during ten (10) seconds of simulation. The voltage rise variations further demonstrates the rationality for further investigations and simulations using the load profile data from 18th April in this dissertation.

3.5 Data for simulation with integrated BESS

To further investigate the grid's response and with the integration of a BESS, another simulation is required using a comprehensive dataset providing information such as the yearly solar PV production based on the irradiance data, air temperature and load profile for the entire year as mentioned before in chapter 3.1. To simplify the BESS simulations, 18th April was selected as the data point to conduct the simulation due to the large difference between peak PV production during the day and low load demand.

As seen in Fig. 3.8, the highest PV production during 0600hrs -1730hrs was 163kW meanwhile the lowest load demand was 20kW. Later in the day, the highest PV production between 1731hrs – 2045hrs was 44kW before gradually reducing to 0kW. The peak load demand was 106.73kW, which occurred at approximately 1930hrs which afterwards, gradually reducing to 19.78kW at 2400hrs.

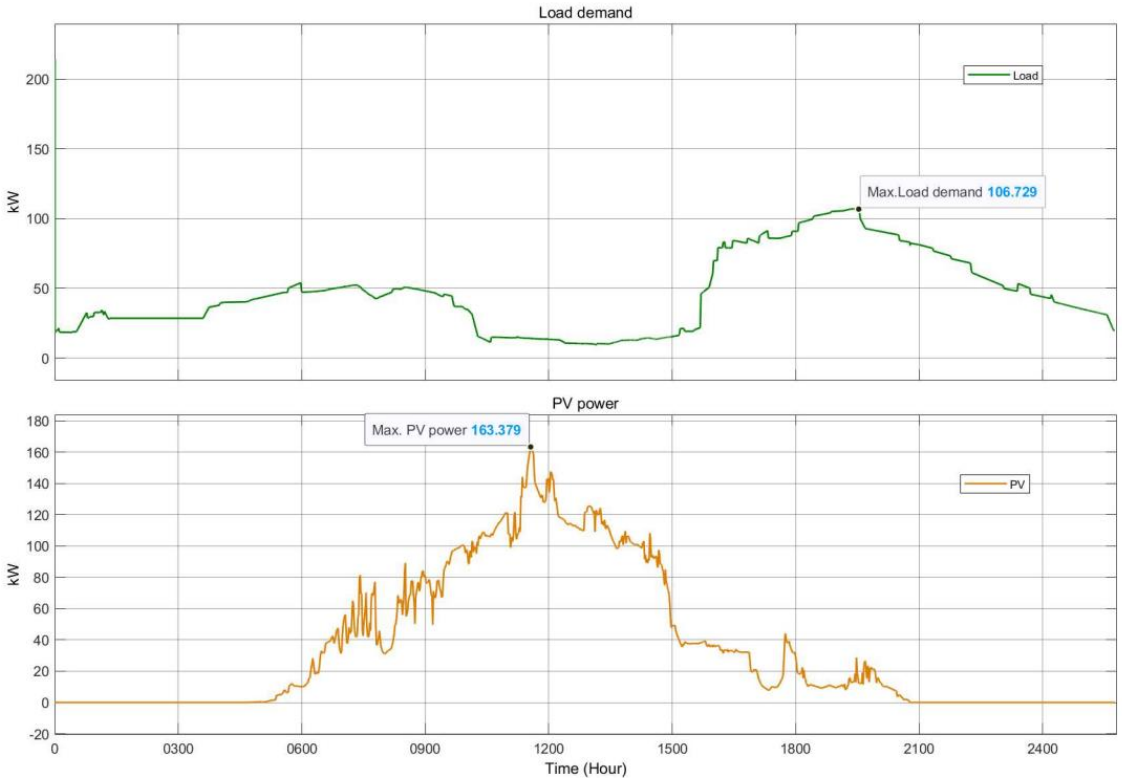

Figure 3.8 POS load demand and PV power on 18th April

Fig. 3.8 illustrates a situation where the PV production during the day is minimally used by the loads, with the excess of the energy being sent back to the external grid contributing to a voltage rise.

3.5.1 Peak shaving control strategy

The method that the author uses in this dissertation to control voltage rise is the peak shaving strategy for battery energy storage systems. This peak shaving control strategy primary focus involves the charging of the BESS by utilizing the surplus PV production and then discharging of the BESS to the supply the loads when the PV power is lower than the load demand during after 1500hr and during the specified peak load demand between 1800hr and 2100hr. The design of this grid with aggregated loads and the integration of a BESS is illustrated in Fig. 3.9. The grid development was inspired by work done from Jonathan Le Sage [47] and the grid was modified with the author's irradiance, load profile data as well as modifications of the grid infrastructure to best represent POS LV grid. The numerical inputs of the transformers, and the BMS of the BESS was modified by the author.

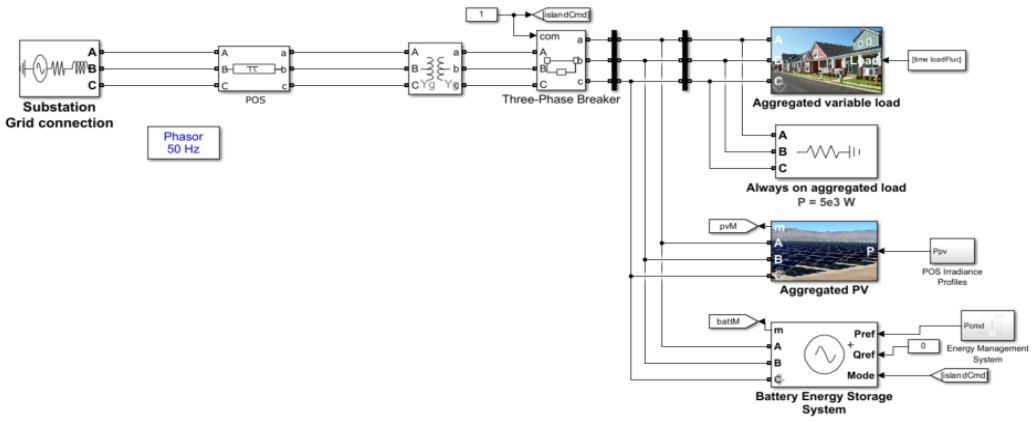

Figure 3.9 POS grid with aggregated loads, PV, and BESS

Using Simulink's state flow, at the start of the charging cycle the BESS will have a SoC of 21%. As the new day starts, the consumer loads utilize the power provided from the transformer and the PV production. As the PV production begins the BESS will commence the charging cycle storing the surplus energy from the PV systems. As the day progresses and the PV production continues to rise, the BESS will store more surplus energy from the PV systems until the BESS reaches 79% SoC. When consumer loads begin to be greater than the PV production, the BMS of the BESS will discharge power to consumer loads and during the specified peak night hours when the load demand is the highest. The steps of this control strategy in State flow are show in the BMS decision flow diagram in appendix F.

3.5.2 Sizing of the BESS

For the sizing of the BESS several parameters are taken into consideration for this dissertation and are listed in Table 3.4 below.

Table 3.4. Parameters for sizing the BESS.

Parameters	Values
Maximum PV production	163.4 kW
Low load demand at max. PV production	20 kW
BESS efficiency	96%
Final SoC	79%
Initial SoC	21%

For determining the power rating of the battery an assumption was made by subtracting the lowest load demand from the maximum PV production during the during the same period. This can give an insight regarding the required maximum power the BESS should be able to store.

Power rating of the BESS = maximum PV production – minimum low load during the same period,

$$= 163.4\ \text{kW} - 20\ \text{kW} = 143.4\ \text{kW} \approx 143\ \text{kW}$$

The author then used peak sun hours as four (4) hours for the peak PV production to calculate the energy capacity requirement of the BESS.

Energy capacity requirement of BESS = Excess PV production · peak sun hours

$$= 143\ \text{kW} \cdot 4\ \text{hours} = 572\ \text{kWh}$$

The overall BESS system efficiency is 96%. However, the calculation for sizing and dimensioning of the BESS will not accommodate for this leading to a reduced capacity.

The operating capacity of the BESS at 100% SoC = 572 kWh · 0.96

$$= 549.12\ \text{kWh} \approx 550\ \text{kWh}$$

Additionally, in this simulation, the BESS will be operating between final SoC of 79% and an initial SoC of 21% as to prolong its lifetime according to reference [46], therefore the effective operating capacity of the BESS will be 58%.

Energy Capacity at 58% = 550 kWh · 0.58

$$= 319\ \text{kWh}$$

Therefore, when the BESS is in full discharging mode the maximum power that is available to be supplied to the loads will be 319 kWh.

3.5.3 Repeatability

The methodology presented in this chapter serves to highlight and list the different steps needed to investigate voltage rise, design of an actual grid in Simulink, sizing of a BESS and the development of a control strategy. The layout of this chapter is written not only to convey the different steps to the reader but to also provide a basis by which this methodology can be repeated and used for real world scenarios such as BESS feasibility studies and grid stability investigations.

4. Results and discussion

4.1 Case study with BESS integration

This chapter presents the main results from the case study for the alleviation of voltage rise using a peak shaving strategy. It closely examines the voltage rise on 18th April ten (10) 16.3 kW PV systems integrated to the grid and presents the results of the reduction of the voltage for that day due to the peak shaving strategy implemented. Lastly, the discussion will conclude this chapter with a deeper analysis of the findings.

4.1.1 Voltage variation

The simulation shows that the voltage rise occurred due to the addition of ten (10) aggregated 16.3 kW PV systems having a total power capacity of approximately 163 kW.

In Fig. 4.0 it showed that the voltage begins to exceed the acceptable limit of 1.10 pu from approximately 1130hrs and reduces below the limit at approximately 1145hrs. This occurs at the same period when the PV systems energy production rises above 152 kW to the maximum PV power of 163kW and then falling below 163 kW as seen in Fig. 4.1.

Also, from Fig. 4.1, the graph shows the magnitude of the reverse flow of power which is the surplus PV power that is fed back to the external grid. Even though the loads use energy from the PV systems, the load demand is not large enough to fully utilize all the energy available and as such, the surplus energy is sent to back to the transformer. Another point to highlight from Fig. 4.1, is that when the PV power is 121 kW at 1100 hrs, the maximum load demand is 18.42 kW. Additionally, when the PV power is 103 kW at 1400hrs, the maximum load demand is 12.79 kW. These large power disparities mostly occur during the periods of 0900hrs to 1500hrs.

In terms of energy, the total energy produced from the PV systems for the day was 845 kWh while the total load energy demand was 1094 kWh. From a broad

view it can be suggested that because the PV energy produced is lower than the load energy demand there should not be voltage rise occurrences.

However, due to the non-linearity of the load demand profile this cannot be achieved.

An example is seen in Fig 4.2 and 4.3, the load energy demand between 1800hrs to 2400hrs consumes 435 kWh which is 39.8 % of total load demand for the day while between the period 0900hrs – 1500hrs uses 100 kWh which is 9 % of total load demand for the day. Additionally, the PV energy produced during 0900hrs – 1500hrs generated 555 kWh which is the largest energy generated for the day and accounted for 50.7 % of total PV production as seen in Fig. 4.3.

This means therefore, that the grid would have to accommodate a substantial energy influx of 455 kwh during a six (6) hour period. The large influx of a reverse flow of energy from the PV system contributes to voltage rise and this transfer of energy dilemma corresponds to the literature in chapter 2.1.4

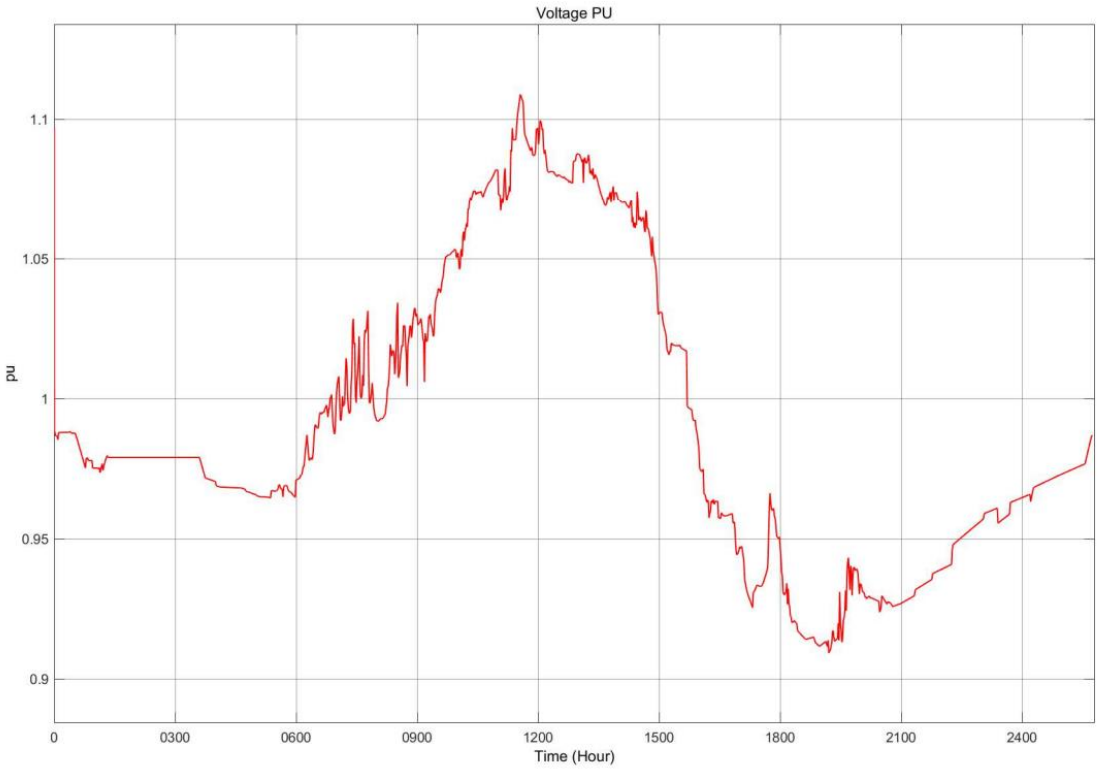

Figure 4.0 Rise in voltage pu with aggregated PV production

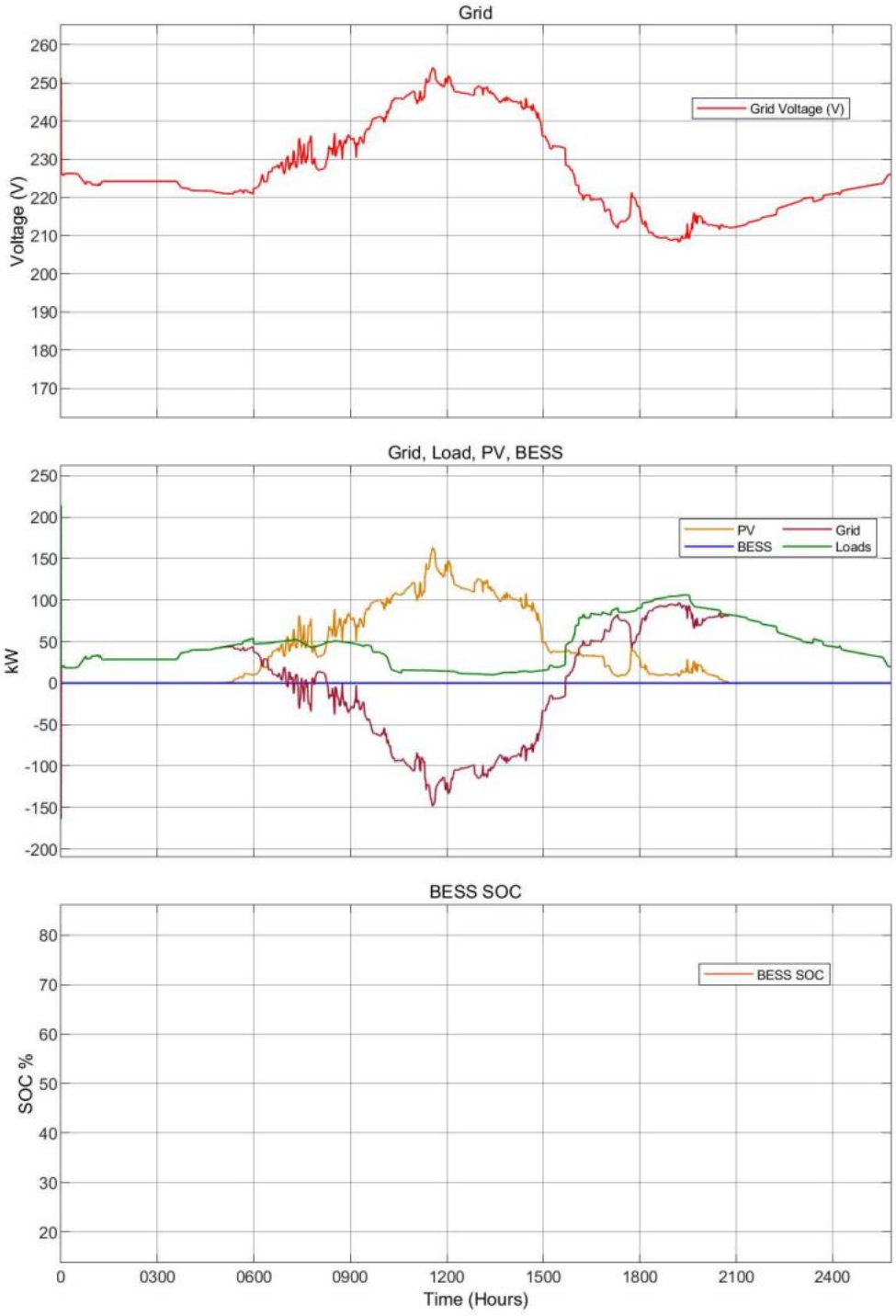

Figure 4.1 Grid voltage, load demand and aggregated PV production

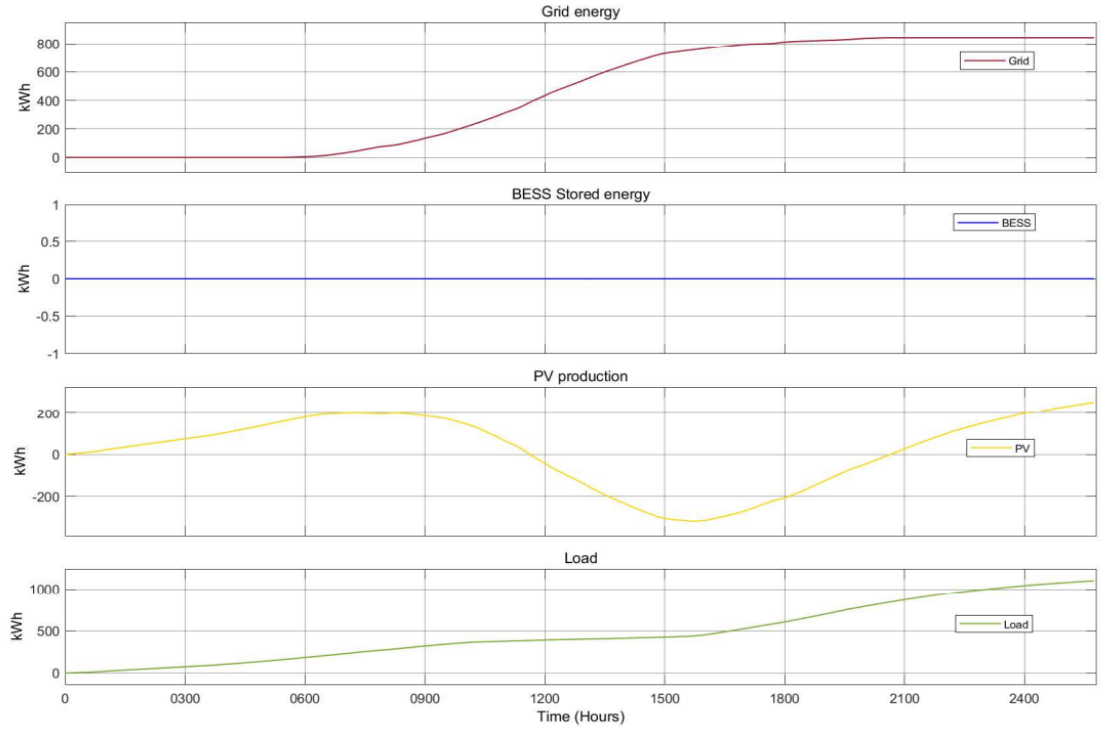

Figure 4.2 Energy utilization without BESS

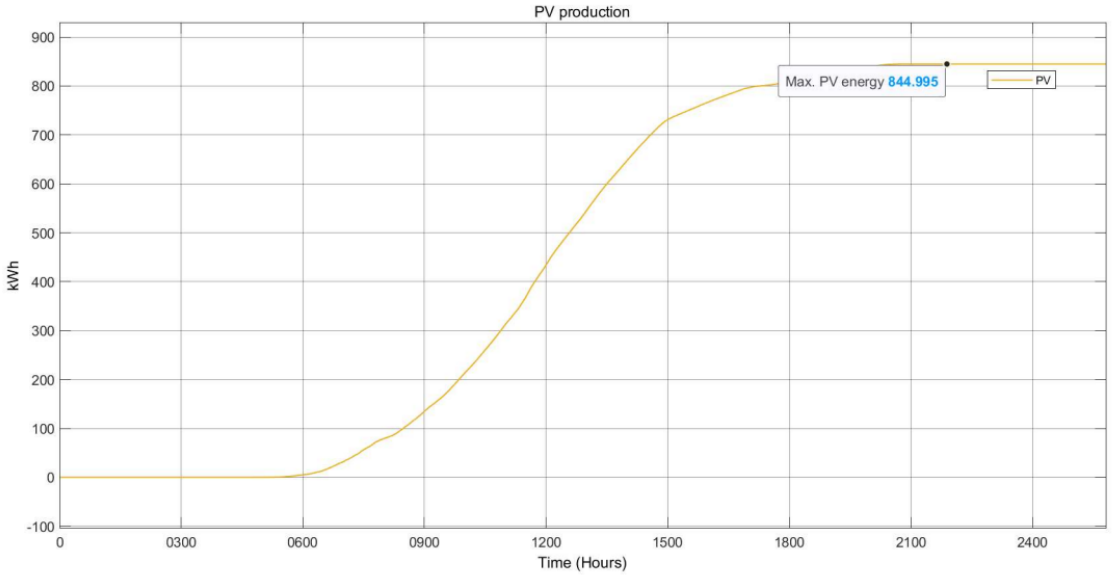

Figure 4.3 PV production

4.1.2 Voltage alleviation using peak shaving

As seen in Fig. 4.4, the BESS begins charging at 21% SoC at 0700 and contributes load shedding. Load shedding not only minimising energy supplied from the grid but also ensures a degree of voltage control at the beginning of the day.

Also shown in Fig. 4.4, when the BESS reaches 79% SoC at approximately 1300hrs, the excess PV power is sent directly to the grid beginning at a maximum power of 107 kW to a minimum of 0k W at 1545hrs when the PV production drops below the power demanded from the loads.

Between 1300hrs and 1544hrs, the BESS is not in use due to the capacity being achieved at 79% SoC. However, the next command for discharging commences at 1545 hrs and during the maximum peak load demand between 1800hrs and 2100hrs.

During the final discharge, the BESS discharges 319kWh of energy which satisfied 79.5 % of the load demand during that same period as seen in Fig. 4.5.

Additionally, it was observed that during the load shedding period between 0700hrs to 0800hrs the energy discharged to the grid was 45.54 kWh reducing the load demand to 8.06 kWh from the transformer. During 0700hrs and 1300hrs the stored excess PV production was approximately 346 kWh which also accounts for 41% of the total PV production. It is important to note that the stored energy is higher than the 319 kWh capacity due to the BESS operating in both charging and discharging modes simultaneously during this period.

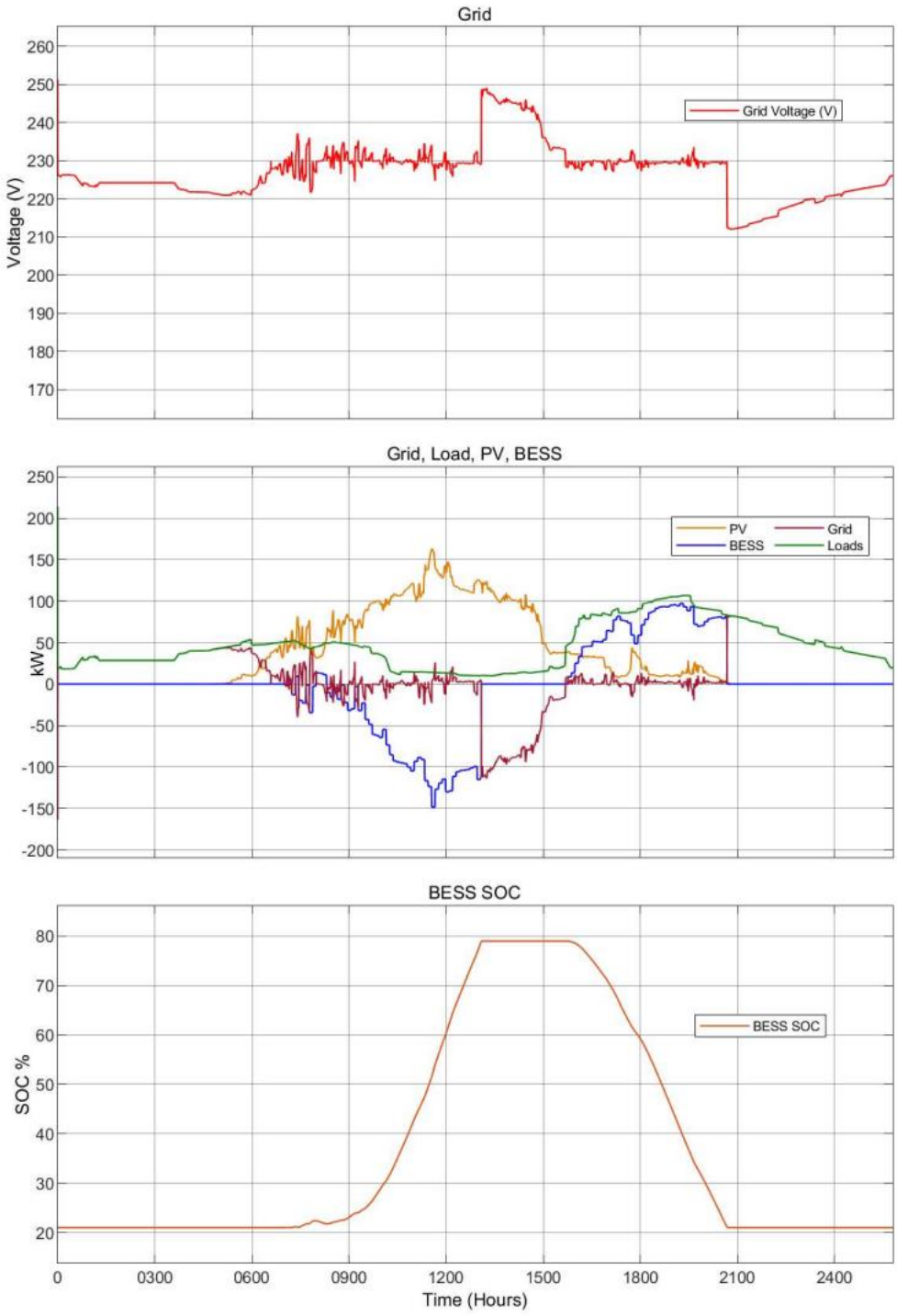

Figure 4.4 Voltage alleviation using the BESS with peak shaving.

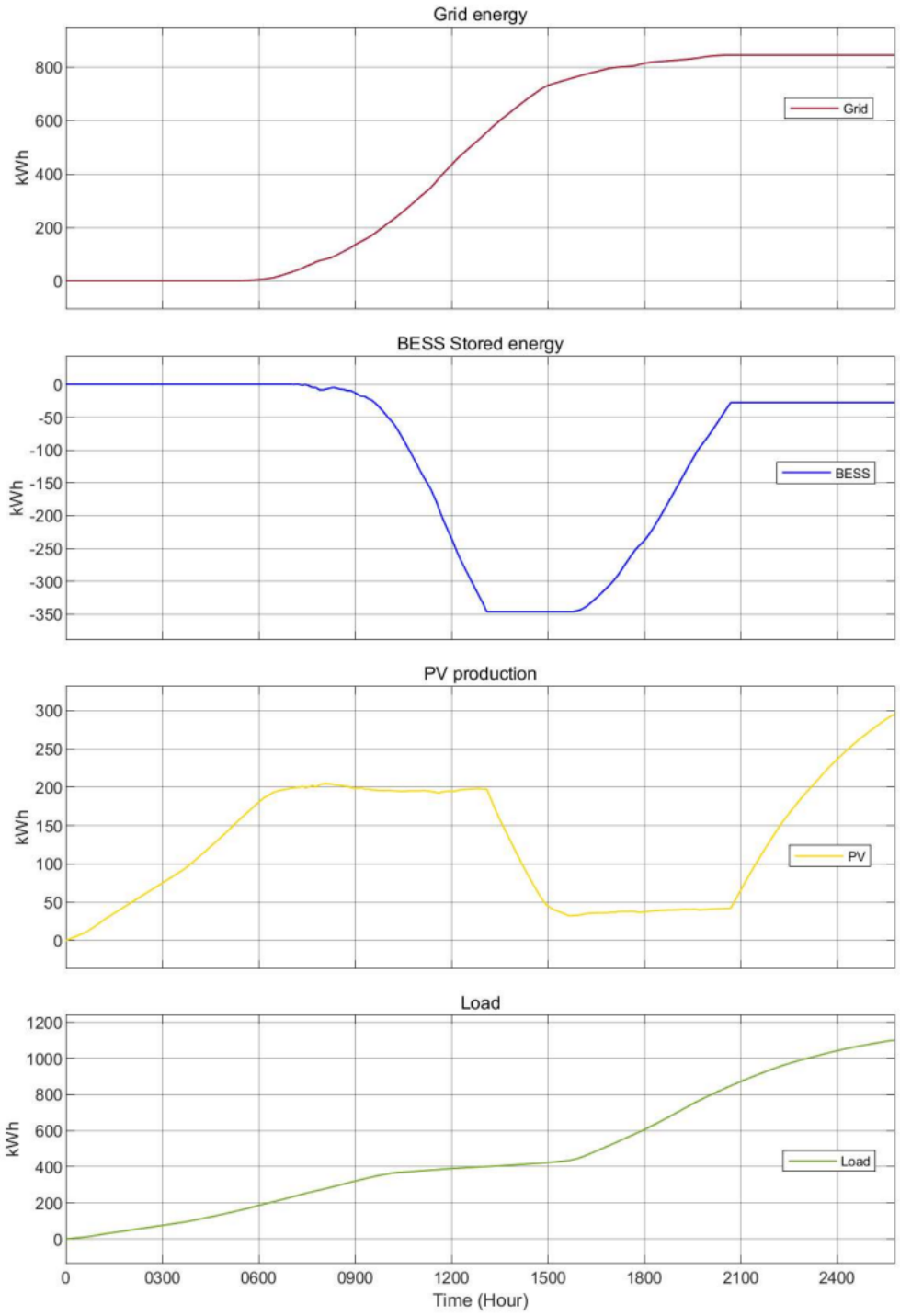

Figure 4.5 Energy utilization with the BESS

As seen in Fig. 4.6, the voltage variations during the day are kept below the limit due to the peak shaving control strategy. By utilizing a BESS with a minimum energy capacity of 572 kWh, it alleviated the voltage rise to an acceptable value of 1.08 pu (248 V) during peak PV production. Additionally, the voltage pu during the peak demand period during the night was slightly improved to 0.92 pu (211 V). There are some important aspects to mention when the results are further analysed that can optimize this strategy in terms of functionality, location, and economics however this will be discussed in the next section.

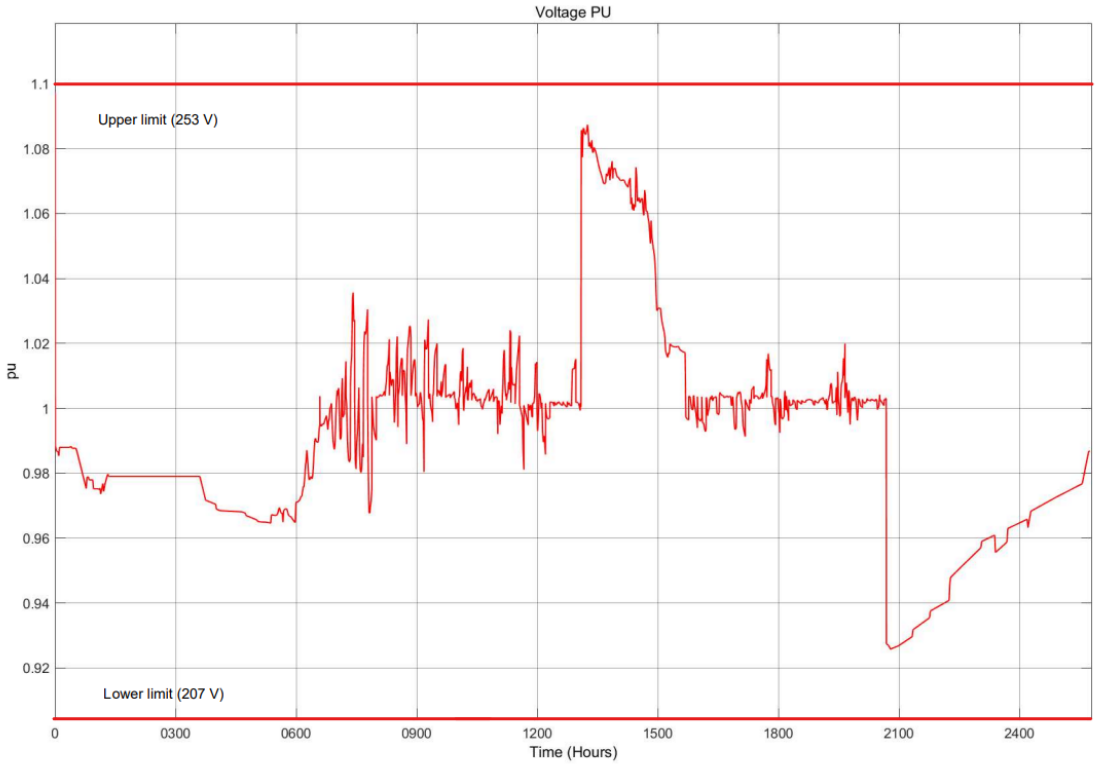

Figure 4.6 Voltage alleviation in pu

4.2 Discussion

4.2.1 R/X ratio impact and BESS location

As mentioned in chapter 2.1.4, a high R/X ratio (above 1) contributes to voltage rise in low voltage grids with a high PV penetration. As seen in chapter 3, Table 3.1, the R/X ratios of two types of overhead lines in the two radials are above 14 while the remaining two types have R/X ratios above 3. All the lines to the consumers on radial A2 have ratios of 14.6.

High R/X ratios also influences the grid without integrated PV systems as a high load demand leads with a high R/X grid leads to a voltage drop. As seen in Fig. 4.8, without the addition of PV systems, the high load demand between 1800hrs – 2000hrs leads to a voltage drop of 0.895pu (206 V) in the grid which is below the minimum acceptable level of 0.90pu (207 V).

These two scenarios in the simulation which shows sharp voltage elevation and reduction, with and without PV systems, illustrates characteristics that are indicative of a weak grid as mentioned in chapter 2.1.4

Fig. 4.7 illustrates the location of the five (5) consumers with PV systems in radial A2 that contribute to voltage rise throughout the entire grid. These consumers all have overhead lines with R/X ratios of 14.6 which suggests that the resistance in the lines are 14.6 times more prominent than reactance, therefore these areas are more susceptible to active power (P) changes than reactive power (Q) changes contributing to voltage rise throughout the grid. This was further supported by the simulations carried out in chapter 3, with figures 3.4, 3.5,3.6 and 3.7 illustrating consumers 16,15,13,14 and 10 all having voltage pu above 1.10pu.

Due to this, the most appropriate location for the BESS to be integrated to the grid, FTM, would be at the point of common connection (PCC) of these five consumers on radial A2 as shown in Fig. 4.7.

This location would ensure that the weakest point in the grid has sufficient voltage support during high PV production thereby successfully maintaining the voltage variation within the acceptable limits issued by FoL.

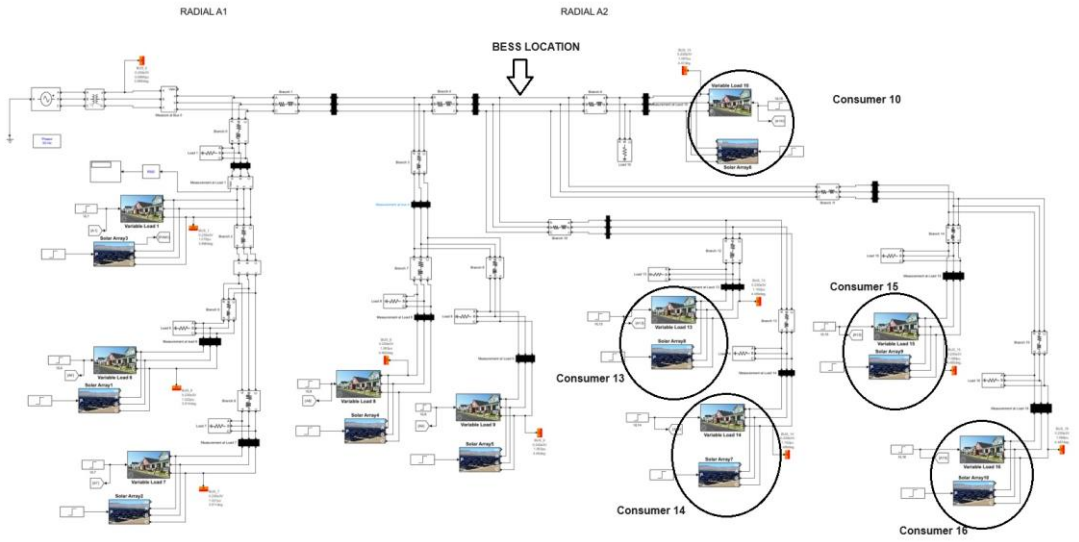

Figure 4.7 Highest overhead line R/X ratio and the location of the proposed BESS

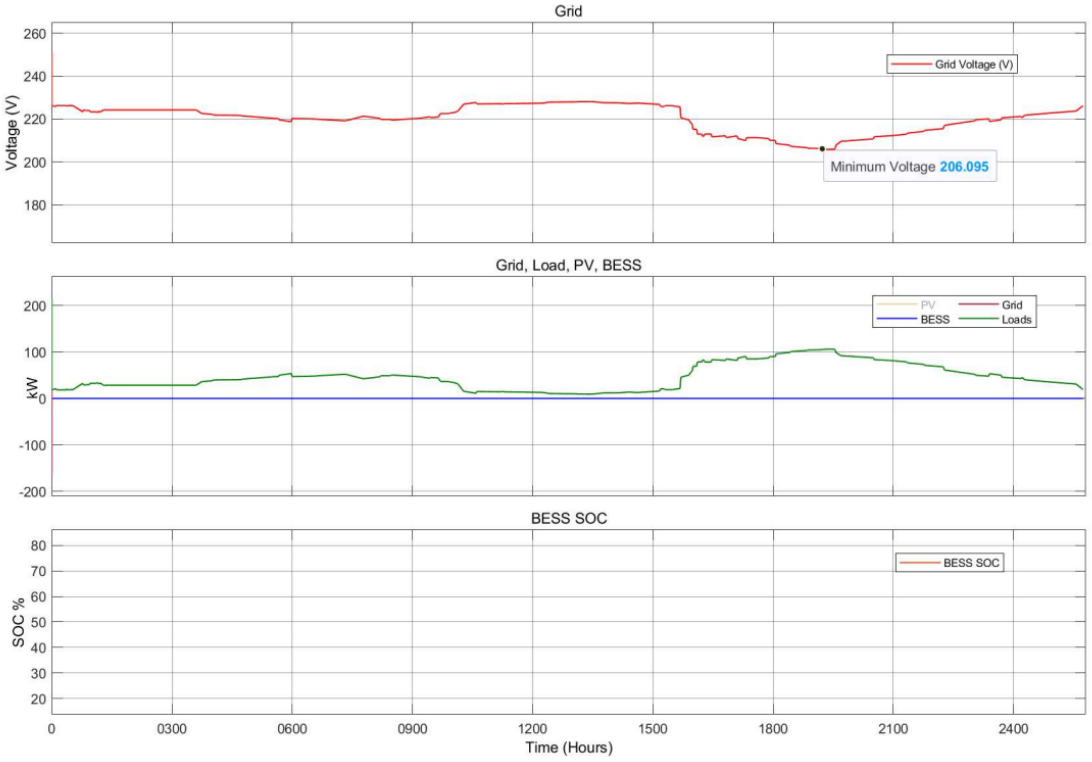

Figure 4.8 Grid without PV and BESS

Table 4.0 R/X ratios of overhead lines to five consumers in radial A2

Consumer	R(Ω)	X (Ω)	R/X ratio
10	0.03	0.00205	14.6
13	0.048	0.00328	14.6
14	0.042	0.00287	14.6
15	0.03	0.00205	14.6
16	0.072	0.00492	14.6

Table 4.1 R/X ratios of lines to consumers in radial A1

Consumer	R(Ω)	X (Ω)	R/X ratio
1	0.1178	0.0079	14.9
6	0.03885	0.01029	3.78
7	0.0222	0.06802721	0.32

4.2.2 Flexibility

The BESS successfully reduced the voltage rise but an additional benefit was the flexibility provided by the battery energy storage system. In order to reduce the magnitude of the reverse flow in the grid it can be seen that the BMS controls the amount of the electricity being supplied by the external grid. This is done by allowing the maximum PV production to supply the loads while the surplus energy is either sent to the BESS for charging to 79% SoC or sent back to the grid. On some occasions, when the PV production experiences an abrupt reduction in production (e.g., due to cloud cover) the external grid is activated to supply the load when the BESS does not have sufficient energy to the supply loads as shown in Fig. 4.9.

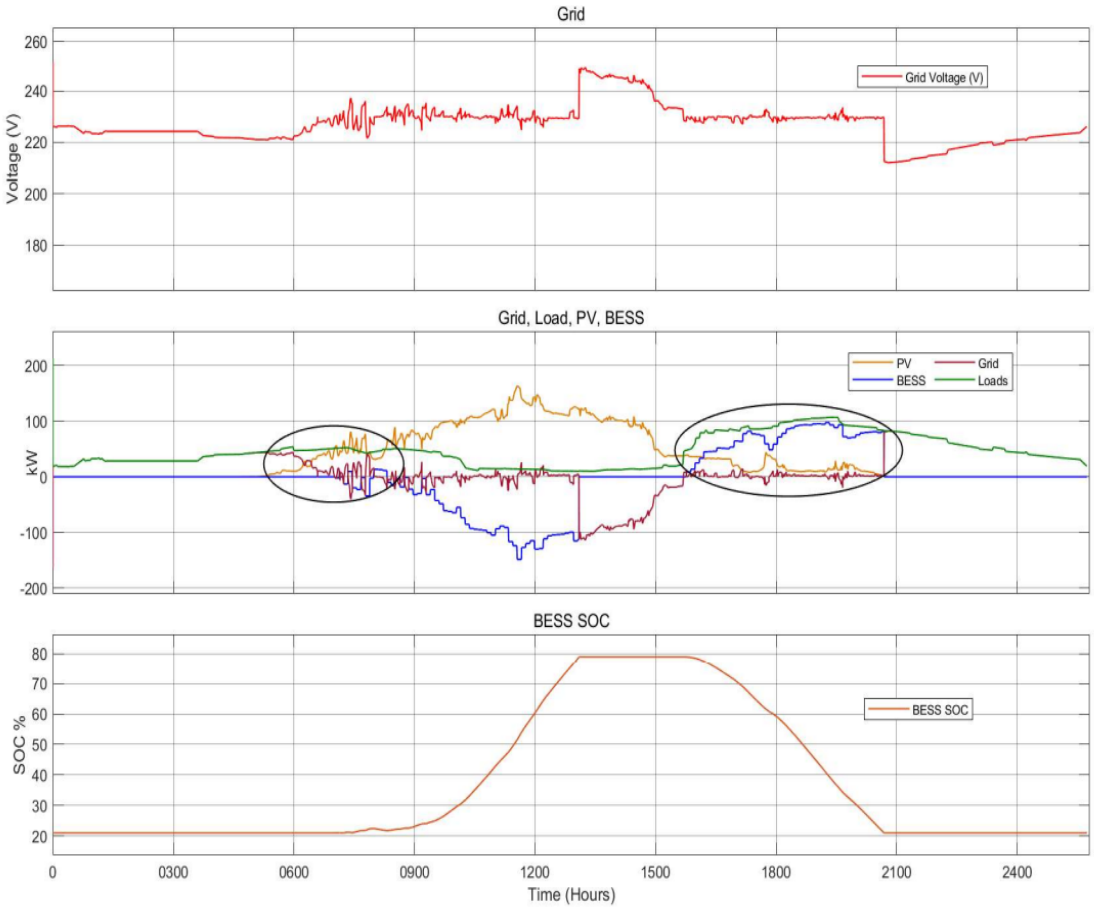

Figure 4.9 External grid utilization

4.2.3 Additional capacity

During the day, the peak shaving method tracks the net PV production throughout the day. In this simulation, 41% of the PV production was stored between the period 0700hrs - 1300hrs while maintaining a voltage of approximately 1 pu as seen in Fig. 4.10. This is beneficial as in Norway there is limited capacity, and there is regulation called connecting by conditions [48] which allows DSOs to conditionally connect with DERs if there is available capacity in the grid. This simulation shows that 6 hours of extra capacity can be available to the grid thereby allowing other production sources to be connected.

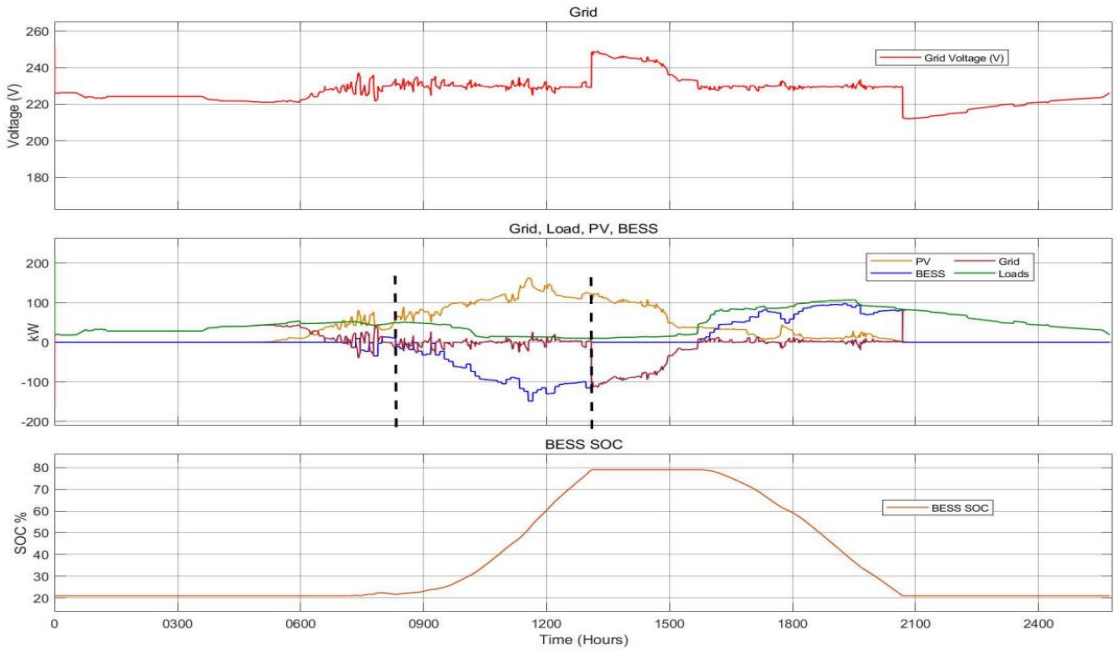

Figure 4.10 Extra capacity during BESS operation

Also, based on a further simulation it was observed that by increasing the capacity of the BESS to a minimum of 857kWh, it fully stored the excess PV production throughout the day. The BESS was in operation from approximately 0700hrs to 2100hrs, maintaining the voltage at approximately 1pu (230 V) for 14 hours. This simulation added further capacity to the external grid as illustrated in appendix G.

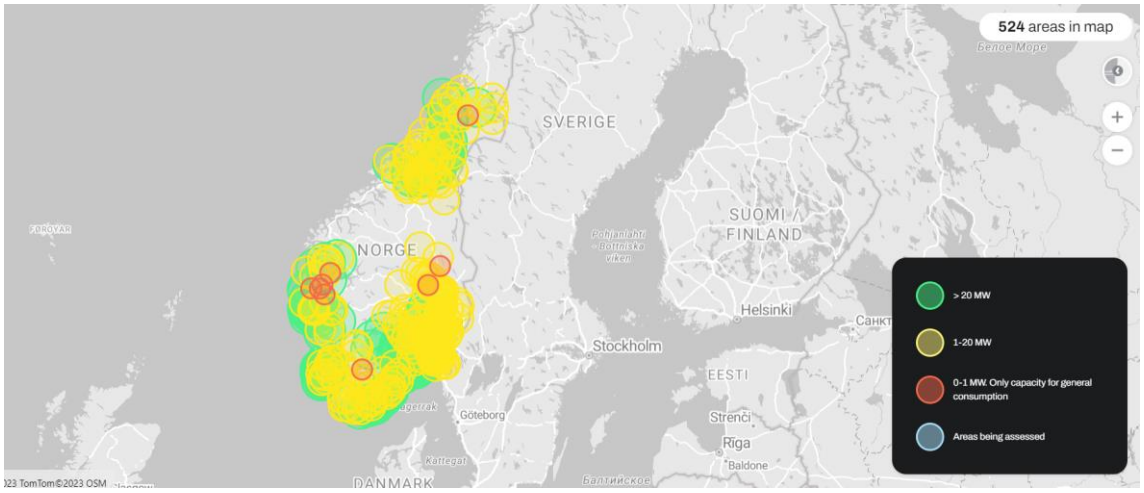

Figure 4.11 Available capacity in Norway for additional production sources

taken from [49]

4.2.4 Advantages and disadvantages

If the BESS employed a simple BMS logic using heuristic parameters such as stipulated charging and discharging times, then the voltage alleviation would have not been sufficient over an extended period but instead only over a fixed time based on the charging logic. This extended period of storing the surplus PV production relative to the load demand is a major advantage of using a peak shaving strategy. Additionally, the peak shaving strategy can be also modified to include electricity spot price information as to not only discharge energy to the load during the peak load demand period but also during a period of the day when the electricity price is the highest, thus showing its versatility. Conversely, using a BESS equipped with a peak shaving BMS requires more sophisticated control systems and maintenance which could contribute to a larger capital cost.

Based on observations from the results a brief table showing the Disadvantages and advantages of peak shaving was developed below in table 4.2.

Table 4.2 Disadvantages and advantages of peak shaving.

Advantages	**Disadvantages**
Real-time optimization	Requires advanced control systems
Enhanced grid stability	Always active therefore requires more maintenance
Versatility	Dependant on real time data

4.2.5 Economics of BESS installation

Based on the results above, a battery of capacity 572 kWh and power rating of 143kW is sufficient to reduce voltage rise to within the acceptable limits. However, the cost of this installation is influenced by current market conditions. For example, the cost of turnkey four-hour energy storage systems is currently priced above 300usd/kWh according to reference [50] thus we can assume a price of 350usd/kWh in 2023 to simplify an assumed cost. Therefore, the cost of a 572 kWh BESS can amount to 200,200usd, which can be deemed expensive.

However, the additional services that the BESS can provide during off peak hours in the night such as reactive power control and frequency stability can provide extra economic opportunities thereby helping offset this high cost.

This BESS intervention is just one method to alleviate voltage rise and it should be compared wholistically to traditional grid re-enforcement costs as to be deemed economically feasible.

5. Conclusion

This dissertation's aim was to model a battery energy storage system to alleviate voltage rise due to a high PV penetration.

The BESS used a peak shaving control strategy and successfully reduced the voltage rise whilst maintaining a grid voltage between 1.08 pu – 0.92 pu. The objective was achieved using a battery energy capacity of 572 kWh with a maximum power rating of 143 kW.

The simulations also showed that a major contributor to voltage rise due to the high PV penetration was the high R/X ratio throughout the grid. Radial A1 had slightly better results due to the near proximity to the transformer and slightly lower overall R/X ratios. Additionally, there were only three (3) consumers being supplied on that radial. Conversely, radial A2 had seven (7) consumers with R/X ratios being higher than that of radial A1 and they were also located further away from the transformer. The grid configuration and characteristics showed that the overhead lines are highly resistive and thus lacked the capacity for receiving additional active power from these PV systems without experiencing overvoltage.

This also suggests that by increasing the transmission capacity of the overhead lines, as done in typical grid re-enforcement methods, would allow the grid to operate more efficiently while being subjected to high PV production.

Alternatively, the simulations illustrated that the grid can be relieved from voltage rise by the BESS storing the net PV production thereby reducing the magnitude of reverse flow in the lines and the transformer. This energy was then used later in the day for load shedding during the peak load demand period, which contributed to a reduced load demand on the overhead lines and transformer as well.

The peak shaving strategy that the BESS employed demonstrated its viability in reducing voltage rise and thus, can be considered as an alternative to traditional grid re-enforcements if deemed financially feasible.

6. Recommendations and future work

Throughout this dissertation, alleviating and reducing the voltage rise was the major focus, however the dynamics of the control strategy was not investigated. As seen in Fig. 4.4 and Fig, 4.5, when the battery reaches a 79% SoC the voltage response was rapid causing a large voltage spike. Although this voltage jump is within the specified limits, this sharp voltage rise can have unwanted effects on some equipment and household appliances. Going forward, implementing a command within the BMS that initiates a slow decrease of charging power when the battery approaches 10% of the final and initial SoC values is recommended thus ensuring a more gradual and controlled voltage variation.

Also, if there is a problem with no capacity being available the BESS can provide an added opportunity to employ an islanded microgrid.

Another aspect to be looked at going forward should be forecasting data. This can be implemented using machine learning to assist and predict the periods in the day when charging and discharging should be done due to weather patterns. With machine learning, the capacity of the battery may be optimized due to the additional information available thereby also potentially reducing cost.

EV charging should be included going forward as this also contributes to additional loading to most low voltage grids. Furthermore, vehicle to load and vehicle to grid technologies are becoming popular which can provide new energy transmission and storage dynamics.

In the future, to simulate more realistic results, these aspects should be investigated and simulated as well.

Bibliography

[1]Elhub, (2023). Solkraft installert effekt, Available at: https://elhub.no/statistikk/installerteffekt/ (Accessed 3 October 2023).

[2] Norges vassdrags- og energidirektorat, (2019). Analyse og Framskrivning av Kraftproduksjon i Norden til 2040 NVE, Available at: https://publikasjoner.nve.no/rapport/2019/rapport2019_43.pdf/ (Accessed 21 September 2023).

[3] Energifakta-Norge, (2019). The Electricity Grid, Available at: https://energifaktanorge.no/en/norsk-energiforsyning/kraftnett/ (Accessed 28 August 2023).

[4] Bremen, L.V., (2010). Large-scale variability of weather dependent renewable energy sources, In Management of weather and climate risk in the energy industry, Dordrecht: Springer, pp. 189-206.

Available at: https://link.springer.com/book/10.1007/978-90-481-3692-6/.

[5] International energy agency, (2023). Solar PV still dominates renewable energy capacity additions, Available at: https://www.iea.org/energy-system/renewables/solar-pv/ (Accessed 18 August 2023).

[6] Norges vassdrags- og energidirektorat, (2022). The Norwegian network structure, Available at:https://www.nve.no/norwegian-energy-regulatory-authority/networkregulation/#:~:text=Network%20structure,distribution%20network%20(22kV%2D240V)/ (Accessed 11 August 2023).

[7] Forskrift om leveringskvalitet i kraftsystemet (Leveringskvalitetsforskriften) 2004.(SI 2004/1557). Available at: https://lovdata.no/dokument/SF/forskrift/2004-11-30-1557/ (Accessed 5 August 2023).

[8] Store Norske Leksikon, (2021). Spenningskvalitet, Available at: https://snl.no/spenningskvalitet/ (Accessed 17 September 2023)

[9] International energy agency, (2021). Norway Energy Policy Review, Available at: https://www.iea.org/reports/norway-2022/ (Accessed 18 September 2023).

[10] Schneider electric, (2003). How to Calculate the Required Capacity kVA Rating or Amperage Capacity for Single and Three Phase Transformers, Available at: https://www.se.com/us/en/faqs/FA101694/ (Accessed 1 October 2023).

[11] Norsk Elektroteknisk Komite, (2022). The road to 230/400V TN-CS, Available at:https://www.nek.no/2022/06/22/veien-til-230-400-v-tn-c-s/ (Accessed 14 September 2023).

[12] Norsk Elektroteknisk Komite, (2022). IT network, a Norwegian phenomenon, Available at:https://www.nek.no/2022/06/22/veien-til-230-400-v-tn-c-s/ (Accessed 14 September 2023).

[13] Lightning and Surge Protection, (2018). Power Supply System (TN-C, TN-S, TN-C-S, TT, IT), Available at: https://www.lsp-international.com/power-supply-system/ (Accessed 22 September).

[14] Verma, P., et al., (2022). Voltage Rise Mitigation in PV Rich LV Distribution Networks Using DC/DC Converter Level Active Power Curtailment Method, *Energies*,**15,** (16), 5901. Available at: https://doi.org/10.3390/en15165901

[15] Nair, D.S. and Rajeev, T., (2022). Impact of Reverse Power Flow Due to High Solar PV Penetration on Distribution Protection System, In Panda, G., Naayagi, R.T.,Mishra, S. Eds., Sustainable Energy and Technological Advancements. Advances in Sustainability Science and Technology, Singapore: Springer, pp. 1-13. Available at: https://doi.org/10.1007/978-981-16-9033-4_1/.

[16] Kenneth, A. P. and Folly, K., (2014). Voltage rise issue with high penetration of grid connected pv, *IFAC Proceedings Volumes*, **47,** (3), pp.4959–4966.

[17] Huang, L., et al., (2021). Impact of Grid Strength and Impedance Characteristics on the Maximum Power Transfer Capability of Grid-Connected Inverters, *Applied Sciences*, **11**, (9) 4288.

[18] Leisse, I., (2013). Efficient Integration of Distribution Generation in Electricity Distribution Networks – Voltage Control and Network Design, Thesis (Ph.D). Lund University.

[19] European Distributed Energy Resources Laboratories, (2013). DERlab activity report. Available at: https://der-lab.net/resources/ (Accessed 13 October 2023).

[20] Unigwe,O., et al., (2017). Economical distributed voltage control in low-voltage grids with high penetration of photovoltaic, *CIRED - Open Access Proceedings Journal*, **2017,** (1), pp.1722–1725.

[21] Li, C., et al., (2018). Optimal OLTC voltage control scheme to enable high solar penetrations. *Electric Power Systems Research,* **160,** (2018), pp.318–326.

[22] De Brabanderee K., et al., (2007). A Voltage and Frequency Droop Control Method for Parallel Inverters, *IEEE Transactions on Power Electronics*, **22**, (4), pp.1107-1115.

[23] Renewable Academy (RENAC), (2003). Frequency and Voltage Regulation in Electrical Grids, Available at: http://docplayer.net/6038884-Regrid-frequency-and-voltage-regulation-in-electrical-grids.html (Accessed 2 November 2023).

[24] Opiyo, N.N., (2018). Droop Control Methods for PV-Based Mini Grids with Different Line Resistances and Impedances. *Smart Grid and Renewable Energy*, **9**, (6), pp.101-112.

[25] Mathworks (2023). Islanded Operation of an Inverter-based Microgrid Using Droop Control Technique, Available at:https://se.mathworks.com/help/sps/ug/power-Microgrid-IslandedOperation-DroopControl.html/ (Accessed 2 November 2023).

[26] L.R.Visser., et al., (2022). Regulation strategies for mitigating voltage fluctuations induced by photovoltaic solar systems in an urban low voltage grid, *International Journal of Electrical Power and Energy Systems,* **137,** (2022), 107695, Available at: https://doi.org/10.1016/j.ijepes.2021.107695

[27] Farivar, M., et al., (2011). Inverter VAR control for distribution systems with renewables, *IEEE International Conference on Smart Grid Communications (SmartGridComm)*,*2011*, Brussels, 17-20 October 2011, pp. 457-462.

[28] Norges vassdrags- og energidirektorat, (2019). Nettkundenes nytte av en oppgradering av lavspenningsnettet, Available at: https://publikasjoner.nve.no/eksternrapport/2019/eksternrapport2019_07.pdf/ (Accessed 13 October 2023).

[29] Olje-og energidepartementet, (2012). Vi bygger Norge - om utbygging av strømnettet, Melding til Stortinget. Volume 14, Available at: https://www.regjeringen.no/no/dokumenter/meld-st-14-20112012/id673807/sec2/ (Accessed on 1 September 2023).

[30] Choi, D., et al., (2021). Li-ion battery technology for grid application, *Journal of Power Sources*, **511**, (2021), 230419, Available at: https://doi.org/10.1016/j.jpowsour.2021.230419

[31] Ibrahim, H., et al., (2008). Energy storage systems-Characteristics and comparisons, *Renewable and Sustainable Energy Reviews*, **12**, (5), pp.1221–1250.

[32] Wu, D., et al., (2015). An energy storage assessment: Using optimal control strategies to capture multiple services, *IEEE Power and Energy Society General Meeting 2015*, Denver, 26-30 July 2015, pp. 1-5.

[33] National Renewable Energy Laboratory, (2023). Cost Projections for Utility-Scale Battery Storage: 2023 Update.

Available at: https://www.nrel.gov/docs/fy23osti/85332.pdf

[34] Yang, Y., et al., (2018). Battery energy storage system size determination in renewable energy systems: A review, *Renewable and Sustainable Energy Reviews*, **91**, (2018), pp.109–125.

[35] Aghamohammadi, M.R. and Abdolahinia, H., (2014). A new approach for optimal sizing of battery energy storage system for primary frequency control of islanded Microgrid, *International Journal of Electrical Power and Energy Systems*, **54**, (2014), pp.325–333.

[36] Zhang, Y.J.A., et al., (2018). Profit-maximizing planning and control of battery energy storage systems for primary frequency control, *IEEE Transactions on Smart Grid*, **9,** (2), pp.712–723.

[37] Rocky Mountain institute, (2015). The Economics of Battery Energy Storage 2015. Available: https://rmi.org/wp-content/uploads/2017/03/RMI-TheEconomicsOfBatteryEnergyStorage-FullReport-FINAL.pdf (Accessed 6 September 2023).

[38] Rana, M.M., et al., (2022). A Comparative Analysis of Peak Load Shaving Strategies for Isolated Microgrid Using Actual Data. *Energies* **15,** (1) 330, Available at: http://dx.doi.org/10.3390/en15010330

[39] Ebrahimi, A. and Hamzeiyan, A., (2023). An ultimate peak load shaving control algorithm for optimal use of energy storage systems, *Journal of Energy Storage*, **73**, (2023), 109055, Available at: https://doi.org/10.1016/j.est.2023.109055/.

[40] Zupančič, J., et al., (2017). Advanced peak shaving control strategies for battery storage operation in low voltage distribution network, *IEEE Manchester PowerTech conference 2017*, Manchester, 18-22 June 2017, pp. 1-6.

[41] Micallef, A., et al., (2022). Utility-Scale Storage Integration in the Maltese Medium-Voltage Distribution Network. *Energies* **15,** (8), 2724, Available at: https://doi.org/10.3390/en15082724

[42] European Commission (2020). SARAH-2 Solar radiation data.

Available at: https://joint-research-centre.ec.europa.eu/photovoltaic-geographical-information-system-pvgis/pvgis-data-download/sarah-2-solar-radiation-data_en (Accessed on 3 September 2023).

[43] Amillo, G., et al., A.M., (2021). Adapting PVGIS to Trends in Climate, Technology and User Needs, *38th European Photovoltaic Solar Energy Conference and Exhibition (PVSEC) 2021,* Brussels, 6-10 September 2021, pp 907 - 911.

[44] Brubæk, M., (2020). Battery Storage as Alternative to Grid Reinforcement in the Low-Voltage Network, thesis (MSc.). Norwegian University of Science and Technology.

[45] Mathworks (2023). Systems-Level Microgrid Simulation from Simple One-Line Diagram, Available at: (https://www.mathworks.com/matlabcentral/fileexchange/67060-systems-level-microgrid-simulation-from-simple-one-line-diagram) (Accessed August 7 2023).

[46] Le Sage, J., (2020). Microgrid Energy Management System (EMS) using Optimization. (https://github.com/jonlesage/Microgrid-EMS-Optimization/releases/tag/v19.1.0), (Accessed August 18 2023).

[47] Collath, N., et al., (2022). Aging aware operation of lithium-ion battery energy storage systems: A review, *Journal of Energy Storage*,**55**, (2022),105634, Available at: https://doi.org/10.1016/j.est.2022.105634 .

[48] Norges vassdrags- og energidirektorat, (2019). Tilknytning av produksjon med vilkår, Available at: https://www.nve.no/reguleringsmyndigheten/regulering/nettvirksomhet/nettilknyt

ning/tilknytningsplikt/tilknytning-av-produksjon-med-vilkaar/ (Accessed 23 October 2023)

[49] Wattapp Norway, (2023). Available capacity in Norway, Available at: https://www.wattapp.no/?baseTimeSeriesKind=actual (Accessed 28 October 2023)

[50] Bloomberg, (2023). Top 10 energy storage trends in 2023, Available at: https://about.bnef.com/blog/top-10-energy-storage-trends-in-2023/ (Accessed 26 October 2023)

[51] Trina Solar (2020). TSM-DE17(II), Available at: https://static.trinasolar.com/sites/default/files/MA_Datasheet_TallmaxM_DE17M(II)_2020C.pdf (Accessed 19 August 2023)

Appendix A. PV system required area.

The PV system in this dissertation has maximum power capacity of 16.3 kWp and modules were manufactured by Trina Solar, with the model number TSM-DE17M(II).

Appendix A.1.0 Peak power and dimensions for TSM-DE17(II) panel

Taken from [51]

Peak power (Wp)	**Area**
455 Wp	2.17 m^2(2102mm x 1040mm)

The number of panels for the PV system is calculated below,

Number of panels = $\frac{16300W}{455Wp}$ = $35.82 \approx 36\, panels$

Therefore, the PV system needs 35 panels to have a capacity of 16 kW.

Required roof surface area = 36 · 2.17 m^2 = 78.12 m^2

Thus, the aggregated surface needed for all ten (10) PV systems is calculated.

78.12 · 10 = 781.2 m^2

Appendix B. Calculating inductive reactance and base impedance.

As stated in section chapter 3, the inductive reactance and impedance values need to be calculated to design the grid in Simulink.

Calculations for overhead lines to consumer 4 are shown below.

Calculating Base impedance:

To begin, a base apparent power (S_{base}) of 1kVa was assumed and the base voltage to the nodes was also assumed to be the grid voltage of 230 V. Base impedance was calculate using equation (B.10),

Base Impedance: $Z_{\mathbf{base}} = \frac{V_{base}^2}{S_{base}}$ (B1.0)

$$= \frac{230^2}{1000} = 52.9\Omega$$

Using node at consumer 4 inductive reactance was calculated using equation B1.1,

Inductive reactance: $L = \frac{X \cdot Z_{\mathbf{base}}}{2 \cdot \pi \cdot 50}$ (B1.1)

$$= \frac{[(0.050 \cdot 0.082)/1000] \cdot 52.9}{2 \cdot \pi \cdot 50} = 6.90e\text{ -}04\ H$$

Appendix C. Variable load demand of consumers

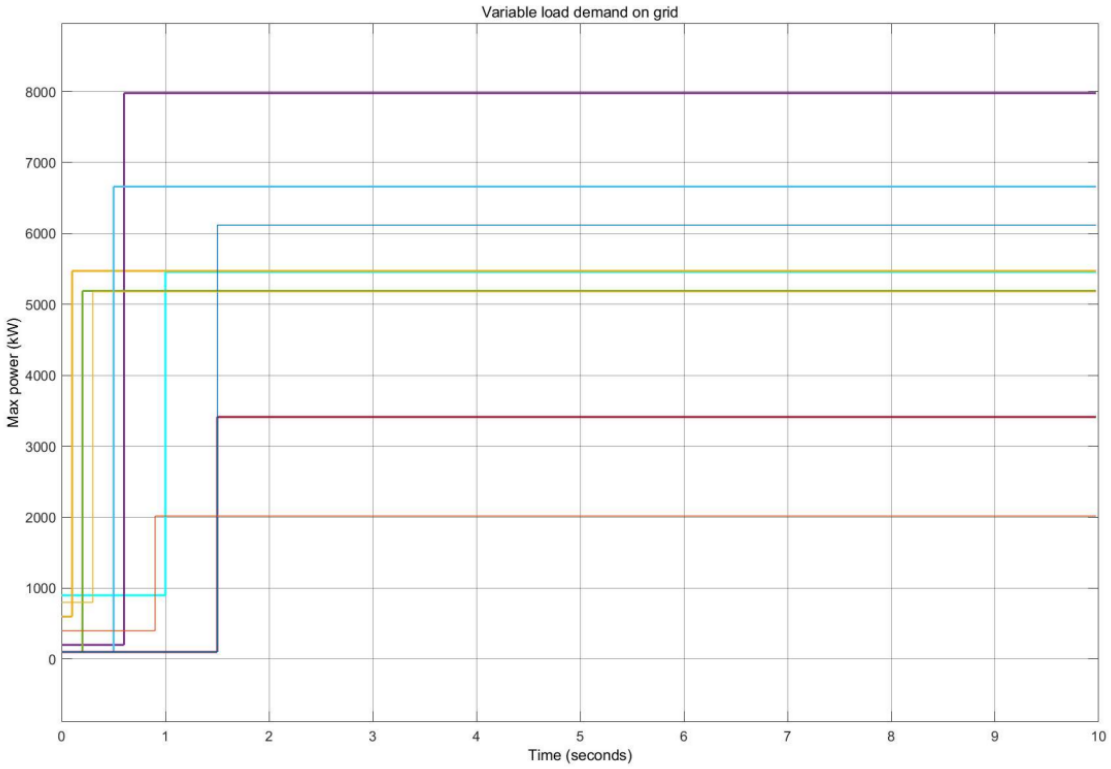

Appendix C 1.0 Variable load demand of consumers

Appendix D. Load flow analysis of consumers with PV systems

	Block name	Block type	Bus type	Bus ID	Vbase (kV)	Vref (pu)	Vangle (deg)	P (MW)	Q (Mvar)	Qmin (Mvar)	Qmax (Mvar)	V_LF (pu)	Vangle_LF (deg)	P_LF (MW)	Q_LF (MVA)
1	Load Flow Bus1	Bus	-	BUS_0	0.2300	1.0000	0	0	0	0	0	1.0153	4.0317	0	0
2	Solar Array9/Simple Solar Inverter	DYN load	PQ	BUS_15	0.2300	1.0000	0	-0.0150	-0.0000	-Inf	Inf	1.1193	3.5475	-0.0150	-0.0000
3	Variable Load 15/Simple Three-Phase Load	DYN load	PQ	BUS_15	0.2300	1.0000	0	0.0055	0.0000	-Inf	Inf	1.1193	3.5475	0.0055	0.0000
4	Load 15	RLC load	Z	BUS_15	0.2300	1.0000	0	0.0001	-0.0020	-Inf	Inf	1.1193	3.5475	0.0001	-0.0025
5	Solar Array10/Simple Solar Inverter	DYN load	PQ	BUS_16	0.2300	1.0000	0	-0.0150	-0.0000	-Inf	Inf	1.1198	3.5434	-0.0150	-0.0000
6	Variable Load 16/Simple Three-Phase Load	DYN load	PQ	BUS_16	0.2300	1.0000	0	0.0052	0.0000	-Inf	Inf	1.1198	3.5434	0.0052	0.0000
7	Load 16	RLC load	Z	BUS_16	0.2300	1.0000	0	0.0001	-0.0020	-Inf	Inf	1.1198	3.5434	0.0001	-0.0025
8	Solar Array3/Simple Solar Inverter	DYN load	PQ	BUS_1	0.2300	1.0000	0	-0.0150	-0.0000	-Inf	Inf	1.0411	4.0092	-0.0150	-0.0000
9	Variable Load 1/Simple Three-Phase Load	DYN load	PQ	BUS_1	0.2300	1.0000	0	0.0061	0.0000	-Inf	Inf	1.0411	4.0092	0.0061	0.0000
10	Load 1	RLC load	Z	BUS_1	0.2300	1.0000	0	0.0001	-0.0020	-Inf	Inf	1.0411	4.0092	0.0001	-0.0022
11	Solar Array2/Simple Solar Inverter	DYN load	PQ	BUS_7	0.2300	1.0000	0	-0.0150	-0.0000	-Inf	Inf	1.0447	3.9910	-0.0150	-0.0000
12	Variable Load 7/Simple Three-Phase Load	DYN load	PQ	BUS_7	0.2300	1.0000	0	0.0052	0.0000	-Inf	Inf	1.0447	3.9910	0.0052	0.0000
13	Load 7	RLC load	Z	BUS_7	0.2300	1.0000	0	0.0001	-0.0020	-Inf	Inf	1.0447	3.9910	0.0001	-0.0022
14	Solar Array1/Simple Solar Inverter	DYN load	PQ	BUS_6	0.2300	1.0000	0	-0.0150	-0.0000	-Inf	Inf	1.0462	3.9847	-0.0150	-0.0000
15	Variable Load 6/Simple Three-Phase Load	DYN load	PQ	BUS_6	0.2300	1.0000	0	0.0020	0.0000	-Inf	Inf	1.0462	3.9847	0.0020	0.0000
16	Load 6	RLC load	Z	BUS_6	0.2300	1.0000	0	0.0001	-0.0020	-Inf	Inf	1.0462	3.9847	0.0001	-0.0022
17	Solar Array4/Simple Solar Inverter	DYN load	PQ	BUS_8	0.2300	1.0000	0	-0.0150	-0.0000	-Inf	Inf	1.0834	4.0566	-0.0150	-0.0000
18	Variable Load 8/Simple Three-Phase Load	DYN load	PQ	BUS_8	0.2300	1.0000	0	0.0067	0.0000	-Inf	Inf	1.0834	4.0566	0.0067	0.0000
19	Load 8	RLC load	Z	BUS_8	0.2300	1.0000	0	0.0001	-0.0010	-Inf	Inf	1.0834	4.0566	0.0001	-0.0012
20	Solar Array5/Simple Solar Inverter	DYN load	PQ	BUS_9	0.2300	1.0000	0	-0.0150	-0.0000	-Inf	Inf	1.0838	4.0630	-0.0150	-0.0000
21	Variable Load 9/Simple Three-Phase Load	DYN load	PQ	BUS_9	0.2300	1.0000	0	0.0034	0.0000	-Inf	Inf	1.0838	4.0630	0.0034	0.0000
22	Load 9	RLC load	Z	BUS_9	0.2300	1.0000	0	0.0001	-0.0010	-Inf	Inf	1.0838	4.0630	0.0001	-0.0012
23	Solar Array6/Simple Solar Inverter	DYN load	PQ	BUS_10	0.2300	1.0000	0	-0.0150	-0.0000	-Inf	Inf	1.1168	3.5729	-0.0150	-0.0000
24	Variable Load 10/Simple Three-Phase Load	DYN load	PQ	BUS_10	0.2300	1.0000	0	0.0052	0.0000	-Inf	Inf	1.1168	3.5729	0.0052	0.0000
25	Load 10	RLC load	Z	BUS_10	0.2300	1.0000	0	0.0001	-0.0010	-Inf	Inf	1.1168	3.5729	0.0001	-0.0012
26	Solar Array8/Simple Solar Inverter	DYN load	PQ	BUS_13	0.2300	1.0000	0	-0.0150	-0.0000	-Inf	Inf	1.1210	3.5070	-0.0150	-0.0000
27	Variable Load 13/Simple Three-Phase Load	DYN load	PQ	BUS_13	0.2300	1.0000	0	0.0080	0.0000	-Inf	Inf	1.1210	3.5070	0.0080	0.0000
28	Load 13	RLC load	Z	BUS_13	0.2300	1.0000	0	0.0001	-0.0020	-Inf	Inf	1.1210	3.5070	0.0001	-0.0025
29	Solar Array7/Simple Solar Inverter	DYN load	PQ	BUS_14	0.2300	1.0000	0	-0.0150	-0.0000	-Inf	Inf	1.1212	3.5117	-0.0150	-0.0000
30	Variable Load 14/Simple Three-Phase Load	DYN load	PQ	BUS_14	0.2300	1.0000	0	0.0055	0.0000	-Inf	Inf	1.1212	3.5117	0.0055	0.0000
31	Load 14	RLC load	Z	BUS_14	0.2300	1.0000	0	0.0001	-0.0020	-Inf	Inf	1.1212	3.5117	0.0001	-0.0025
32	Three-Phase Programmable Voltage Source	Vprog	swing	'1'	11.0000	1.0000	0	0	0	-Inf	Inf	1.0000	0	-0.0890	-0.0121

Appendix D 1.0 Load flow analysis results in simulink

Appendix E. Overview of Voltages with and without PV installations

Appendix E 1.0 Voltages of all consumers with and without PV systems

Location	Voltage pu without PV systems	Voltage pu with PV systems
Consumer 1	0.976	1.03
Consumer 6	0.974	1.03
Consumer 7	0.974	1.03
Consumer 8	0.936	1.07
Consumer 9	0.937	1.07
Consumer 10	0.909	1.11
Consumer 13	0.907	1.11
Consumer 14	0.906	1.11
Consumer 15	0.903	1.11
Consumer 16	0.904	1.11

Appendix F. Peak shaving command process in Simulink's state flow

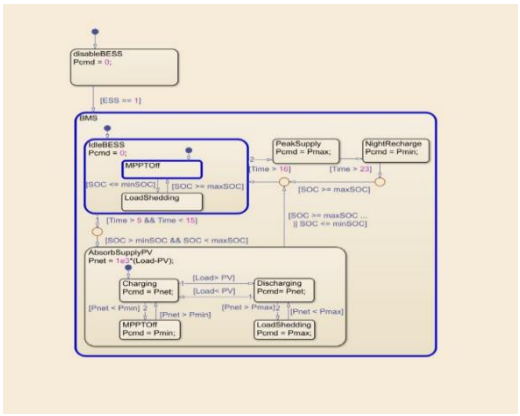

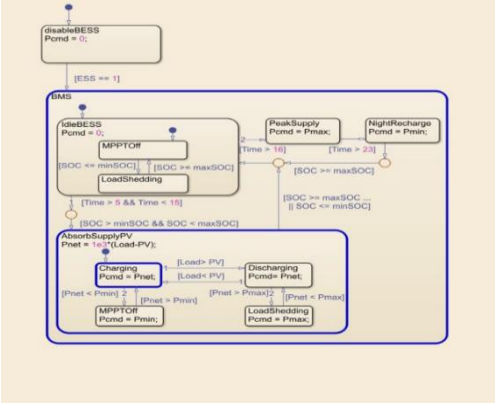

1. At the beginning of the day the BESS is idle as the SoC is 21% and the net power is 0, therefore no command has been activated. The first command is given to charge when the PV production is > than the loads and the time is >0500hrs. The second command is given to discharge as the PV production < than the load demand, initiating load shedding.

2. As the day progresses the PV production > the load demand which initiates the charging command until the battery reaches 79% SoC.

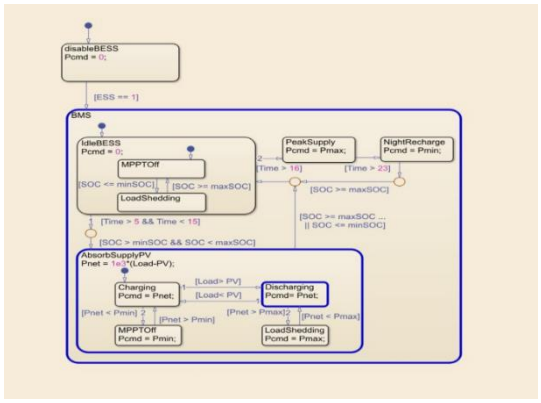

3. The discharging command begins when PV< Pmax and after 1600. As the load demands increases, the BESS discharges more energy to the loads.

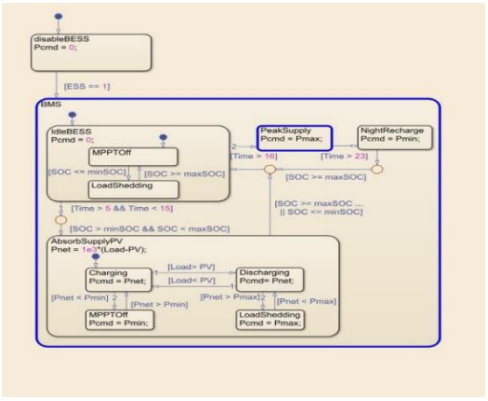

4. The discharging command continues during the peak supply/peak load period initiating the command to discharge until the BESS reaches 21% SoC. Night recharge is command is not activated but can be modified to do if needed.

Appendix F 1.0 Peak shaving command process

Appendix G. Simulation using BESS with added capacity.

An additional simulation was done incrementally increasing the capacity by 25kWh to examine the response. Based on this simple methodology and without modifying the command strategy and keeping the final and initial SoC at 79% and 21% respectively, it was found that the minimum capacity at which the BESS can fully support the loads, while reducing the grid voltage occurred at 857 kWh.

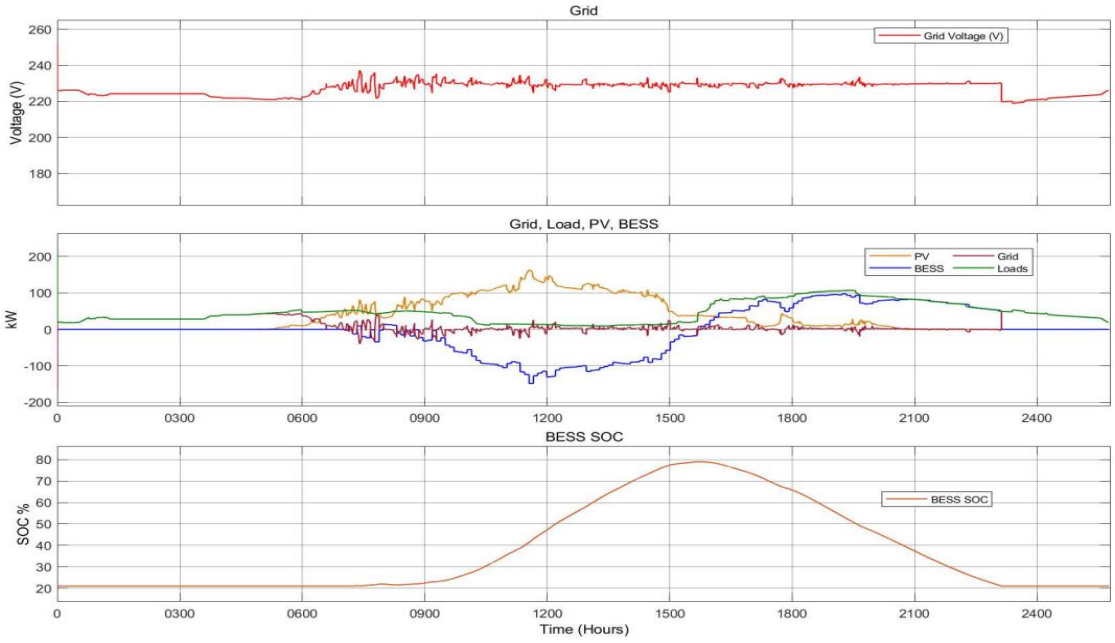

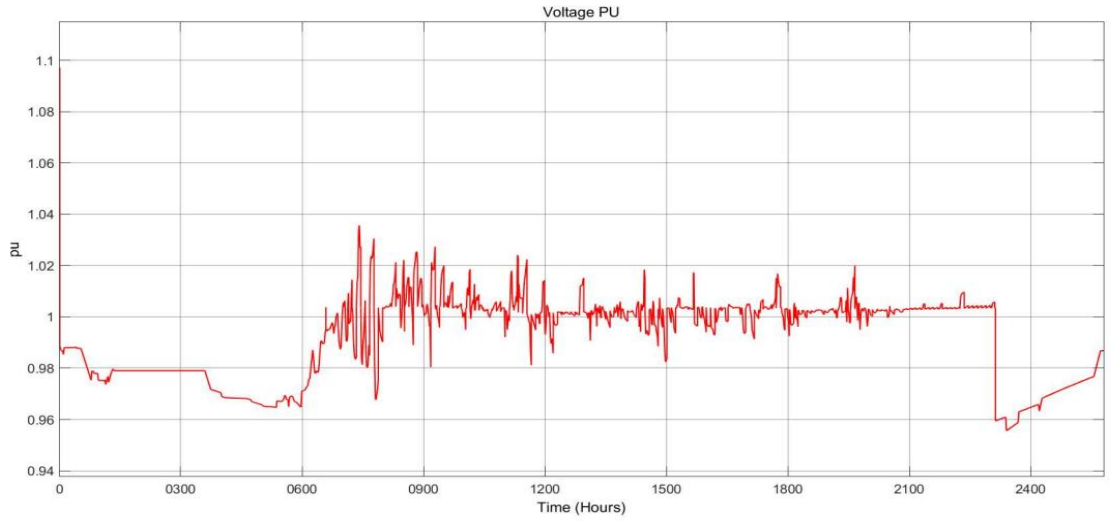

Appendix G 1.0 Voltage alleviation with an 857 kWh BESS

Appendix H. MATLAB code for BESS simulation

```
load time.mat;
load loaddata.mat;
load costData.mat;
load clearday.mat;
load cloudyDay.mat
load N.mat
load Pload.mat


% Microgrid Settings
panelArea = 781.2;   % Area of PV Array [m^2]
panelEff = 0.20;     % Efficiency of Array
loadBase = 5e3;   % Base Load of Microgrid [W]

BattCap = 572;     % Energy Storage Rated Capacity [kWh]
batteryMinMax.Pmin = -143e3;    % Max Discharge Rate [W]
batteryMinMax.Pmax = 143e3;     % Max Charge Rate [W]

% Online optimization parameters
FinalWeight = 1;    % Final weight on energy storage
timeOptimize = 5;    % Time step for optimization [min]
timePred = 20;        % Predict ahead horizon [hours]

% Compute PV Array Power Output
POSPpv = panelArea*panelEff*pvsarah2;
POSPpv = panelArea*panelEff*pvsarah2;

% Select Load Profile
loadSelect = 3;
loadFluc = loadData(:,loadSelect);

% Battery SOC Energy constraints (keep between 21%-79% SOC)
battEnergy = 3.6e6*BattCap;
batteryMinMax.Emax = 0.79*battEnergy;
batteryMinMax.Emin = 0.21*battEnergy;

% Setup Optimization time vector
optTime = timeOptimize*60;
stepAdjust = (timeOptimize*60)/(time(2)-time(1));
N = numel(time(1:stepAdjust:end))-1;
tvec = (1:N)'*optTime;

% Horizon for "sliding" optimization
M = find(tvec > timePred*3600,1,'first');

numDays = 2; % Repeat data for end of day forcasts
loadSelect = 3;
clearPpvVec = panelArea*panelEff*repmat(clearDay(2:stepAdjust:end),numDays,1);
for loadSelect = 1:4
    loadDataOpt(:,loadSelect) = repmat(loadData(2:stepAdjust:end,loadSelect),numDays,1) + loadBase;
end
C = repmat(costData(2:stepAdjust:end),numDays,1);

CostMat = zeros(N,M);
PpvMat = zeros(N,M);
PloadMat = zeros(N,M);

% Construct forecast vectors for optimization (N x M) matrix
for i = 1:N
    CostMat(i,:) = C(i:i+M-1);
```

```
    PpvMat(i,:) = clearPpvVec(i:i+M-1);
    PloadMat(i,:) = loadDataOpt(i:i+M-1,loadSelect);
end
```

Appendix I. Risk Assessment Form

[Not produced as no field work was undertaken during this project. All work was done by using a Hp EliteBook laptop, Intel Core i7 and the work was mostly done at home or at my office at work.]